

Renormalized mean-field theory of the neutron scattering in cuprate superconductors

Jan Brinckmann¹ and Patrick A. Lee²

¹*Institut für Theorie der Kondensierten Materie, Universität Karlsruhe, D-76128 Karlsruhe, Germany*

²*Department of Physics, Massachusetts Institute of Technology, Cambridge, Massachusetts 02139*

(6 July 2001)

The magnetic excitation spectrum of the t - t' - J -model is studied in mean-field theory and compared to inelastic neutron-scattering (INS) experiments on $\text{YBa}_2\text{Cu}_3\text{O}_{6+y}$ (YBCO) and $\text{Bi}_2\text{Sr}_2\text{CaCu}_2\text{O}_{8+\delta}$ (BSCCO) superconductors. Within the slave-particle formulation the dynamical spin response is calculated from a renormalized Fermi liquid with an effective interaction $\sim J$ in the magnetic particle-hole channel. We obtain the so-called “41 meV resonance” at wave vector (π, π) as a collective spin-1 excitation in the d-wave superconducting state. It appears sharp (undamped), if the underlying Fermi surface is hole-like with a sufficient next-nearest-neighbor hopping $t' < 0$. The double-layer structure of YBCO or BSCCO is not important for the resonance to form. The resonance energy ω_{res} and spectral weight at optimal doping come out comparable to experiment. The observed qualitative behavior of ω_{res} with hole filling is reproduced in the underdoped as well as overdoped regime. A second, much broader peak becomes visible in the magnetic excitation spectrum if the 2D wave-vector is integrated over. It is caused by excitations across the maximum gap, and in contrast to the resonance its energy is almost independent of doping. At energies above or below ω_{res} the commensurate resonance splits into incommensurate peaks, located off (π, π) . Below ω_{res} the intensity pattern is of “parallel” type and the dispersion relation of incommensurate peaks has a negative curvature. This is in accordance with recent INS experiments on YBCO.

PACS numbers: 71.10.Fd, 74.25.Ha, 74.72.Bk, 75.20.Hr

I. INTRODUCTION

The study of magnetic excitations plays an important rôle in the ongoing attempt to understand the physics of High-Temperature Superconductors. A key observation is the so-called “41 meV resonance” from inelastic neutron scattering (INS) experiments [1–4]. In superconducting optimally doped $\text{YBa}_2\text{Cu}_3\text{O}_{6+y}$ (YBCO_{6+y}) a sharp peak occurs in the magnetic structure factor at the antiferromagnetic (AF) wave vector $\mathbf{q} = (\pi, \pi)$ and energy 41 meV. It appears resolution limited in energy and therefore is described as an (undamped) δ -peak. This is not expected for a d-wave superconductor, since the density of states is finite and the resonance energy $\omega_{res} \approx 40$ meV is not small compared to $2\Delta^0$, with the maximum gap $\Delta^0 \sim 30 \dots 40$ meV [5]. When temperature is raised through $T_c \approx 93$ K into the normal state, the resonance vanishes. The main effect of underdoping [6–9] on the resonance in the superconducting state is a continuous reduction of its energy, as far as $\omega_{res} \approx 24$ meV for the most underdoped samples $T_c \approx 50$ K. The resonance also gains spectral weight with underdoping. In contrast to the optimally doped case it persists into the normal state above T_c , where the pseudo-gap regime is found. Recently a resonance has also been observed [10–12] in $\text{Bi}_2\text{Sr}_2\text{CaCu}_2\text{O}_{8+\delta}$ (BSCCO_{8+\delta}). Its energy 43 meV in the optimally doped sample is comparable to the case of YBCO. If experiments on YBCO and BSCCO are put together, ω_{res} seems to follow T_c , i.e., it is maximal for optimal doping and is reduced in under- as well as overdoped compounds [9,11].

In this paper we report theoretical calculations of the

magnetic excitation spectrum in YBCO and BSCCO. Our starting point is the doped Mott insulator, described by the t - J -model. We follow the standard procedure of introducing auxiliary “slave” particles and treating the problem in mean-field theory. In the resulting effective theory the d-wave superconducting phase and the pseudo-gap regime of underdoped systems are represented as spin-charge separated states. The dynamical magnetic susceptibility is obtained from a Fermi liquid of strongly renormalized quasi particles that carry the spin. The “41 meV resonance” is interpreted as a collective spin-1 excitation, it arises from a particle-hole (ph) bound state of these quasi particles. We find results in good qualitative agreement with the neutron-scattering experiments. In particular, the behavior of the resonance energy ω_{res} with hole filling is reproduced for underdoped as well as overdoped systems, and we obtain reasonable absolute values for ω_{res} and spectral weight of the resonance at optimal doping. Our findings are discussed in detail from the doping dependent band structure of the quasi particles.

The concept of the resonance coming from a ph-bound state has been put forward in several studies using “slave”-particle schemes for t - J and Hubbard models [13–17], a Hubbard-operator technique [18], approaches based on BCS theory [19–23], and self-consistent treatments of spin fluctuations in the Hubbard model (FLEX) [24–26] or spin-fermion model [27,28]. In the SO(5) approach [29,30], on the other hand, the resonance is a result of a bound state in the spin-triplet particle-particle (pp) channel, which couples to the magnetic ph-channel in the superconducting state. In Ref. [31] we studied

the contribution from the pp-channel within the present slave-particle scheme and concluded that it cannot give rise to a resonance below $2\Delta^0$ unless unreasonable parameters are used. A similar conclusion has been given in Ref. [32].

The resonance is connected to incommensurate structures in wave-vector space. Above and below the resonance energy ω_{res} a splitting of the single peak at $\mathbf{q} = (\pi, \pi)$ into four peaks slightly displaced from (π, π) is observed [33–38]. When energy is raised from ω_{res} these follow a dispersion $\omega(\mathbf{q})$ similar to AF spin waves; however, the peaks are very broad. Below ω_{res} four well separated peaks are visible, which move away from (π, π) with decreasing energy and hence are described by an ‘upside-down’ dispersion. Interestingly these peaks are displaced from the AF wave vector in direction of the $(\pi, 0)$ or $(0, \pi)$ points, rotated from the nodal directions by 45° . This is the same “parallel” type of incommensurability as is known from the $\text{La}_{2-x}\text{Sr}_x\text{CuO}_{4+y}$ (LSCO) family of compounds [39,40], where it has been brought into connection to the so-called “stripes”. In the present work we do not consider the possibility of a combined ordering of spin and charge into quasi one-dimensional (stripe-like) structures. Nevertheless, below the resonance energy we obtain an incommensurate pattern of parallel type. This is due to a “dynamic nesting” mechanism in the superconducting state that enhances the intensity at these particular points in wave-vector space. The dispersion relations of incommensurate peaks are traced back to two particle-hole excitation thresholds that vary differently with wave-vector.

Recently the magnetic response has also been studied by averaging the neutron-scattering data over the 2D Brillouin zone [8,34,41]. Besides the resonance, the resulting local magnetic excitation spectrum $\text{Im}\chi_{2D}(\omega)$ shows a second, broad feature at an energy above the resonance, which depends only weakly on the doping level. Within our calculation this feature is naturally explained from particle-hole excitations across the maximum d-wave gap Δ^0 . Their energy $\omega_{hump} \lesssim 2\Delta^0$ comes out almost independent of doping.

The paper is organized as follows: In Sections II to IV the mean-field theory for the t - t' - J -model is derived and some basic implications are reviewed. The magnetic resonance at the AF wave vector (π, π) is considered in Section V for a single CuO_2 plane. Section VI presents results for the magnetic response in wave-vector space. We consider the crossover from commensurate to incommensurate response and the dispersion of incommensurate neutron peaks. In Section VII we take into account that YBCO and BSCCO are actually bi-layer materials with two coupled CuO_2 planes per unit cell. The splitting of the susceptibility into two modes is calculated. The single-layer model considered in the previous sections serves as an effective model for the odd (“acoustic”) mode, where the resonance is observed. In this section

we also discuss the above-mentioned local susceptibility $\text{Im}\chi_{2D}(\omega)$. A summary is given in Section VIII.

Some of the results have been presented briefly in Refs. [31,42]. Work of other authors is further referenced in the respective sections.

II. MODEL AND MEAN-FIELD THEORY

We study the t - J -model on a simple square lattice of Cu-3d orbitals for each of the two CuO_2 layers in YBCO or BSCCO :

$$H = - \sum_{\nu, \nu', \sigma} t_{\nu\nu'} \tilde{c}_{\nu\sigma}^\dagger \tilde{c}_{\nu'\sigma} + \frac{1}{2} \sum_{\nu, \nu'} J_{\nu\nu'} \vec{S}_\nu \vec{S}_{\nu'} . \quad (1)$$

In the subspace with no doubly occupied orbitals, the electron operator on a Cu-lattice site ν is denoted $\tilde{c}_{\nu\sigma}$ with spin index $\sigma = \pm 1$; \vec{S}_ν is the spin-density operator. A Cu-site is specified through $\nu \equiv [i, l]$, where $i = 1 \dots N_L$ indicates the Cu-position within one CuO_2 -plane and $l = 1, 2$ selects the layer in the bi-layer sandwich. $t_{\nu\nu'}$ denotes the effective intra- and inter-layer Cu-Cu-hopping matrix elements, and $J_{\nu\nu'}$ the antiferromagnetic super exchange .

To deal with the constraint of no double occupancy, the standard auxiliary-particle formulation is used,

$$\tilde{c}_{\nu\sigma} = b_\nu^\dagger f_{\nu\sigma} . \quad (2)$$

The fermion $f_{\nu\sigma}^\dagger$ creates a singly occupied site (with spin σ), the “slave” boson b_ν^\dagger an empty one out of the (unphysical) vacuum $b_\nu|0\rangle = f_{\nu\sigma}|0\rangle = 0$. The constraint now takes the form

$$Q_\nu = b_\nu^\dagger b_\nu + \sum_\sigma f_{\nu\sigma}^\dagger f_{\nu\sigma} = 1 . \quad (3)$$

Using (3), local operators can be written in fermions, in particular the particle and spin density read

$$n_\nu = \psi_\nu^\dagger \psi_\nu , \quad \vec{S}_\nu = \frac{1}{2} \psi_\nu^\dagger \vec{\tau} \psi_\nu \quad (4)$$

Here spinors $\psi_\nu = \begin{pmatrix} f_{\nu\uparrow} \\ f_{\nu\downarrow} \end{pmatrix}$, $\psi_\nu^\dagger = \begin{pmatrix} f_{\nu\uparrow}^\dagger \\ f_{\nu\downarrow}^\dagger \end{pmatrix}$ have been introduced, with Pauli matrices $\vec{\tau}$ and $\vec{h} \equiv 1$.

In order to derive a mean-field theory the constraint (3) is relaxed to its thermal average $\langle Q_\nu \rangle = 1$. Together with the number x of doped holes per Cu-site, it fixes the fermion and boson densities to

$$(1-x) = \langle \psi_\nu^\dagger \psi_\nu \rangle , \quad x = \langle b_\nu^\dagger b_\nu \rangle . \quad (5)$$

These are adjusted by chemical potentials μ^b, μ^f . Using a coherent-state path integral the partition function is now represented by the action

$$S = S^0 + S^t + S^J + S^h \quad (6)$$

with

$$\begin{aligned}
S^0 &= \int_0^\beta d\tau \sum_\nu \{ \bar{b}_\nu (\partial_\tau - \mu^b) b_\nu + \bar{\psi}_\nu (\partial_\tau - \mu^f) \psi_\nu \} \\
S^t &= - \int_0^\beta d\tau \sum_{\nu, \nu'} t_{\nu\nu'} \bar{\psi}_\nu \psi_{\nu'} \bar{b}_{\nu'} b_\nu \\
S^J &= \int_0^\beta d\tau \frac{1}{2} \sum_{\nu, \nu'} J_{\nu\nu'} \bar{S}_\nu \vec{S}_{\nu'} \quad , \quad S^h = - \int_0^\beta d\tau \sum_\nu \vec{h}_\nu \vec{S}_\nu
\end{aligned}$$

A magnetic source-field $\vec{h} \equiv \vec{h}_\nu(\tau)$ has been added here, $\beta \equiv 1/k_B T$.

A mean-field decomposition of the interaction terms S^t, S^J is achieved via Feynman's variational principle [43] for the free energy F ,

$$\beta F \leq \Psi[\tilde{S}] \quad , \quad \Psi[\tilde{S}] = \langle S - \tilde{S} \rangle - \ln \tilde{Z} \quad (7)$$

The effective action \tilde{S} determines $\tilde{Z} = \int D[\psi, \bar{\psi}, b, \bar{b}] \exp(-\tilde{S})$ and thermal averages

$$\langle \hat{O} \rangle = \frac{1}{\tilde{Z}} \int D[\psi, \bar{\psi}, b, \bar{b}] \exp(-\tilde{S}) \hat{O}$$

For \tilde{S} we make the quadratic ansatz

$$\begin{aligned}
\tilde{S} &= S^0 + \int d1 d2 \left\{ \bar{\psi}_1 \mathbf{T}_{12}^f \psi_2 \right. \\
&\quad \left. + \bar{b}_1 T_{12}^b b_2 + (\bar{\psi}_1 \mathbf{A}_{12} \bar{\psi}_2 + h.c.) \right\} \\
&\quad - \int d1 \vec{m}_1 \vec{S}_1
\end{aligned} \quad (8)$$

with a shorthand notation $1 \equiv (\nu_1, \tau_1)$, $\int d1 \equiv \sum_{\nu_1} \int_0^\beta d\tau_1$ collecting site ν and time τ indices. \mathbf{T}_{12}^f and \mathbf{A}_{12} are matrices in spin space, e.g., $\mathbf{A}_{12} \equiv A_{12}^{\sigma_1 \sigma_2} \equiv A_{\nu_1 \nu_2}^{\sigma_1 \sigma_2}(\tau_1, \tau_2)$. \tilde{S} consists of quadratic terms for fermions and bosons, which represent all possible mean-field decouplings of the interactions S^t and S^J .

The expectation value $\langle S - \tilde{S} \rangle$ in Eq. (7) is calculated using Wick's theorem, and from the vanishing variation $\delta \Psi[\tilde{S}] = 0$ we obtain equations for the self-consistent parameters,

$$T_{12}^b = -t_{12} \langle \bar{\psi}_2 \psi_1 \rangle \quad (9a)$$

$$T_{12}^{f \sigma \sigma'} = -t_{12} \langle \bar{b}_2 b_1 \rangle \delta_{\sigma \sigma'} \quad (9b)$$

$$-J_{12} \frac{1}{4} \sum_{\mu=1}^3 \langle (\tau_\mu^T \bar{\psi}_2)^{\sigma'} (\tau_\mu \psi_1)^\sigma \rangle$$

$$A_{12}^{\sigma \sigma'} = -J_{12} \frac{1}{8} \sum_{\mu=1}^3 \langle (\tau_\mu \psi_1)^\sigma (\tau_\mu \psi_2)^{\sigma'} \rangle \quad (9c)$$

$$\vec{m}_1 = \vec{h}_1 - \int d2 J_{12} \langle \vec{S}_2 \rangle \quad (9d)$$

τ_μ denotes a Pauli matrix, τ_μ^T its transpose. The effective hopping T^b of bosons as well as the first contribution to the hopping T^f of fermions stem from the decoupling of $\langle S^t \rangle$ in Eq. (7). The Heisenberg term $\langle S^J \rangle$ is factorized through Wick's theorem into contributions to the local magnetic field \vec{m} , the fermion's hopping T^f and pairing amplitude A . These correspond to analyzing S^J in the direct particle-hole (ph) channel of fermions, the exchange ph, and the particle-particle channel, respectively [44]. Further below, when the source field \vec{h} is set to zero, these will be restricted to a Resonating Valence-Bond (RVB) amplitude $T_{\nu\nu'}^f \sim \langle \bar{f}_{\nu\uparrow} f_{\nu'\uparrow} \rangle$ and spin-singlet pairing $A_{\nu\nu'} \sim \langle f_{\nu\uparrow} f_{\nu'\downarrow} \rangle$.

The approximate free energy is the functional Ψ at its stationary point, $\beta F^{appr} = \Psi[\tilde{S}^{stat}]$, with the action \tilde{S}^{stat} given by Eq. (8) and Eqs. (9). The dynamical magnetic susceptibility then follows with $\delta \Psi[\tilde{S}^{stat}] / \delta \vec{h}_1 = -\langle \vec{S}_1 \rangle$ as

$$\vec{\chi}_{12} = - \frac{\delta^2 \Psi[\tilde{S}^{stat}]}{\delta \vec{h}_1 \delta \vec{h}_2} = \frac{\delta}{\delta \vec{h}_1} \langle \vec{S}_2 \rangle = \int d3 \frac{\delta \langle \vec{S}_2 \rangle}{\delta \vec{m}_3} \frac{\delta \vec{m}_3}{\delta \vec{h}_1}$$

Using Eq. (9d) we obtain the usual 'RPA-like' expression; in a matrix notation it reads

$$\chi = [1 + J \chi^{irr}]^{-1} \chi^{irr} \quad (10)$$

The irreducible part is identified as

$$\vec{\chi}_{12}^{irr} = \frac{\delta \langle \vec{S}_2 \rangle}{\delta \vec{m}_1} = \langle \vec{S}_1 \vec{S}_2 \rangle^{conn} + \left(\frac{\delta \langle \vec{S}_2 \rangle}{\delta \vec{m}_1} \right)_{impl} \quad (11)$$

The 1st term on the r.h.s. comes from the \vec{m} which appears explicitly in $\langle \vec{S}_2 \rangle$ through \tilde{S} , Eq. (8). For a vanishing source field $\vec{h} = 0$ it is given by the unrenormalized fermion bubble contained in Fig. 1. Since the operator \vec{S} involves only fermions, no boson excitation occur in χ^{irr} . The 2nd term in Eq. (11) stands for all contributions from the implicit \vec{m} -dependence of $\langle \vec{S}_2 \rangle$ through the other mean-field parameters T^b, T^f, A . Using Eqs. (9a-9c), it gives rise to vertex corrections. These are shown in Fig. 1 (bottom).

In the following we set $\vec{h} = 0$ and consider paramagnetic phases $\vec{m} = 0$, which are symmetric with respect to lattice translations within a CuO_2 -layer and exchange of the layers. In going to wave-vector space, the site index $\nu \equiv [i, l]$, with in-plane site $i = 1 \dots N_L$ and layer index $l = 1, 2$ is replaced by the wave-vector $p \equiv (\mathbf{k}, p_z)$. That is,

$$f_{i l \sigma} = \frac{1}{\sqrt{2N_L}} \sum_k e^{i(k_x i_x + k_y i_y)} \sum_{p_z=0, \pi} e^{i p_z l} f_{p \sigma}$$

and similar for boson operators. Here \mathbf{k} runs over the usual 2D Brillouin zone, and $p_z = 0, \pi$ corresponds to even, odd linear combination of layer orbitals.

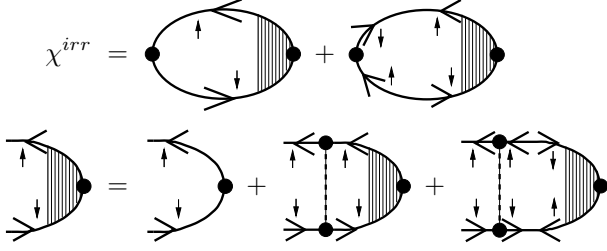


FIG. 1. **Top:** Irreducible part χ^{irr} for vanishing source field $\vec{h} = 0$. Full lines are fermion Green's functions, boson excitations do not enter χ^{irr} at mean-field level. **Bottom:** Bethe-Salpeter equation for the vertex function in χ^{irr} , dashed lines stand for the Heisenberg interaction J . The bare vertex (i.e., the unrenormalized bubble) represents $\langle \vec{S}_1 \vec{S}_2 \rangle^{conn}$ in Eq. (11).

The exchange interaction is decomposed as

$$J_{\nu\nu'} \equiv J_{ij}^{ll'} = \delta_{ll'} J \delta_{\langle i,j \rangle} + (1 - \delta_{ll'}) J^\perp \delta_{ij} \quad (12)$$

It consists of an intra-layer component J for nearest neighbors $\langle i, j \rangle$ and an inter-layer coupling J^\perp for $i = j$. Thus the pairing A of fermions, Eq. (9c), involves an intra-layer part, which we restrict to singlet pairing with d-wave symmetry and equal amplitude and phase in both layers: $\langle f_{l i \uparrow} f_{l i + \hat{x} \downarrow} \rangle = -\langle f_{l i \uparrow} f_{l i + \hat{y} \downarrow} \rangle$, $l = 1, 2$. A contains as well an inter-layer amplitude $\langle f_{1 i \uparrow} f_{2 i \downarrow} \rangle$. In p -space Eq. (9c) then becomes $A_{12}^{\sigma\sigma'} \rightarrow A^{\sigma\sigma'}(p) = \sigma \delta_{-\sigma' \sigma} \Delta_p$, with the gap function

$$\Delta_p = \frac{\Delta^0}{2} [\cos(k_x) - \cos(k_y)] + \Delta^{\perp 0} e^{ip_z} \quad (13)$$

and the maximum in-plane and inter-plane gap $\Delta^0 = \frac{2}{3} J \Delta$, $\Delta^{\perp 0} = \frac{3}{8} J^\perp \Delta^\perp$,

$$\hat{\Delta} = \langle f_{1 i \uparrow} f_{1 i + \hat{x} \downarrow} \rangle - \langle f_{1 i \downarrow} f_{1 i + \hat{x} \uparrow} \rangle \quad (14a)$$

$$\hat{\Delta}^\perp = \langle f_{1 i \uparrow} f_{2 i \downarrow} \rangle - \langle f_{1 i \downarrow} f_{2 i \uparrow} \rangle \quad (14b)$$

As will be explained at the end of this section, in the interesting range of temperature and hole filling x the bosons may be treated as almost condensed. That is, the hopping rate $\langle \bar{b}_\nu b_{\nu'} \rangle \approx \langle \bar{b}_\nu b_\nu \rangle = x$ is independent of ν, ν' and given by the hole density x via Eq. (5). The first term in the fermion hopping Eq. (9b) becomes $-t_{\nu\nu'} \langle \bar{b}_\nu b_{\nu'} \rangle \rightarrow -x t_{\nu\nu'}$. It describes the propagation of fermions with the small probability x of finding an empty site. The second term in Eq. (9b) involves induced hopping amplitudes on nearest-neighbor bonds, which we assume equal in amplitude and phase on each bond within a layer (uniform RVB), $\langle \bar{f}_{l i \uparrow} f_{l i + \hat{x} \uparrow} \rangle = \langle \bar{f}_{l i \uparrow} f_{l i + \hat{y} \uparrow} \rangle$, $l = 1, 2$. The fermion hopping Eq. (9b) now turns into $T_{12}^{f \sigma\sigma'} \rightarrow T^{f \sigma\sigma'}(p) = \delta_{\sigma\sigma'} T_p^f$,

$$T_p^f = -2\tilde{t} [\cos(k_x) + \cos(k_y)] - 4\tilde{t}' \cos(k_x) \cos(k_y) - \tilde{t}^\perp(\mathbf{k}) e^{ip_z} \quad (15)$$

with

$$\tilde{t} = x t + \frac{3}{8} J \hat{\chi}, \quad \tilde{t}' = x t' \quad (16)$$

$$\tilde{t}^\perp(\mathbf{k}) = x t^\perp(\mathbf{k}) + \frac{3}{8} J^\perp \hat{\chi}^\perp$$

and

$$\hat{\chi} = \langle \bar{f}_{1 i \uparrow} f_{1 i + \hat{x} \uparrow} \rangle + \langle \bar{f}_{1 i \downarrow} f_{1 i + \hat{x} \downarrow} \rangle \quad (17a)$$

$$\hat{\chi}^\perp = \langle \bar{f}_{1 i \uparrow} f_{2 i \uparrow} \rangle + \langle \bar{f}_{1 i \downarrow} f_{2 i \downarrow} \rangle \quad (17b)$$

For the bare hopping elements we assumed a nearest and next-nearest neighbor overlap t and t' within a layer, and an inter-layer [45,46] hopping $t^\perp(\mathbf{k}) = 2t^\perp [\cos(k_x) - \cos(k_y)]^2 + t_0^\perp$. For bosons the effective hopping is derived similarly, $T_{12}^b \rightarrow T_p^b$. The result is given at the end of this section.

The mean-field Hamiltonian Eq. (8) now reads

$$\tilde{S} = \int_0^\beta d\tau \sum_p \left\{ \bar{b}_p (\partial_\tau + \Omega_p) b_p + \sum_\sigma \bar{f}_{p\sigma} (\partial_\tau + \varepsilon_p) f_{p\sigma} + [\Delta_p (\bar{f}_{p\uparrow} \bar{f}_{-p\downarrow} - \bar{f}_{p\downarrow} \bar{f}_{-p\uparrow}) + h.c.] \right\} \quad (18)$$

It consists of free bosons with dispersion $\Omega_p = T_p^b - \mu^b$ and BCS-fermions with $\varepsilon_p = T_p^f - \mu^f$ and gap function Eq. (13). After Bogoliubov transformation we obtain 'quasi-fermion' energies $E_p = \sqrt{\varepsilon_p^2 + \Delta_p^2}$, and the mean-field equations (14), (17) become

$$\begin{pmatrix} \hat{\chi} \\ \hat{\chi}^\perp \end{pmatrix} = -\frac{1}{2N_L} \sum_p \begin{pmatrix} \gamma(\mathbf{k})/2 \\ e^{ip_z} \end{pmatrix} \frac{\varepsilon_p}{E_p} \tanh(\beta E_p/2) \quad (19a)$$

$$\begin{pmatrix} \hat{\Delta} \\ \hat{\Delta}^\perp \end{pmatrix} = \frac{1}{2N_L} \sum_p \begin{pmatrix} \varphi(\mathbf{k})/2 \\ e^{ip_z} \end{pmatrix} \frac{\Delta_p}{E_p} \tanh(\beta E_p/2) \quad (19b)$$

$$x = \frac{1}{2N_L} \sum_p \frac{\varepsilon_p}{E_p} \tanh(\beta E_p/2) \quad (19c)$$

with phase factors $\gamma(\mathbf{k}) = \cos(k_x) + \cos(k_y)$, $\varphi(\mathbf{k}) = \cos(k_x) - \cos(k_y)$. The last equation is the particle number constraint (5).

The magnetic susceptibility Eq. (10) is isotropic in spin-space for $\vec{h} = \vec{m} = 0$, and takes the usual form

$$\chi_p(\omega) = \frac{\chi_p^{irr}(\omega)}{1 + J_p \chi_p^{irr}(\omega)} \quad (20)$$

where J_p is obtained from Eq. (12) as

$$J_p = 2J [\cos(q_x) + \cos(q_y)] + e^{ip_z} J^\perp \quad (21)$$

In experiment the magnetic response χ^{meas} is measured as a function of the wave vector (\mathbf{q}, q_z) , which spans the 3D Brillouin zone of the bi-layer material. It is given by [47]

$$\chi^{meas}(\mathbf{q}, q_z, \omega) = \quad (22)$$

$$(g\mu_B)^2 \left[\chi_p(\omega)|_{p_z=0} \cos^2\left(\frac{d}{2}q_z\right) + \chi_p(\omega)|_{p_z=\pi} \sin^2\left(\frac{d}{2}q_z\right) \right]$$

with $p = (\mathbf{q}, p_z)$. d denotes the spacing of layers in the double-layer. The even ($p_z = 0$) and odd ($p_z = \pi$) mode susceptibilities correspond to the in-phase and anti-phase combination of spin fluctuations in the planes. For the irreducible part Eq. (11) we take the bare bubble $\chi_{\nu\nu'}^{irr}(\tau, \tau') = \langle S_\nu^z(\tau) S_{\nu'}^z(\tau') \rangle^{conn}$. The vertex corrections depicted in the bottom of Fig. 1 can be safely ignored. As we have discussed in Ref. [31] they have no significant effect in the interesting energy range $0 \leq \omega \leq 2\Delta^0$. With the effective Hamiltonian Eq. (18) we get the expression known from BCS theory

$$\chi_p^{irr}(\omega) = \frac{1}{2N_L} \sum_{\bar{p}} \sum_{s,s'=\pm 1} \quad (23)$$

$$\frac{1}{8} \left[1 + ss' \frac{\varepsilon\varepsilon' + \Delta\Delta'}{EE'} \right] \frac{f(s'E') - f(sE)}{\omega + sE - s'E' + i0_+}$$

Here $\varepsilon \equiv \varepsilon_{\bar{p}}$, $\varepsilon' \equiv \varepsilon_{\bar{p}+p}$, and similar for Δ , E . f denotes the Fermi function.

We close this section with a remark on Bose condensation. From Eq. (9a) the boson dispersion is $\Omega_p = -2t\tilde{\chi}[\cos(k_x) + \cos(k_y)] - \mu^b$, where for simplicity $t' = t^\perp = 0$. Near the band minimum $k = 0$ this becomes $\Omega_p \approx \bar{\Omega} + k^2/2m^b$, with the mass $1/m^b = 2t\tilde{\chi}$. From the solution of Eqs. (19) we get values around $\tilde{\chi} \approx 0.4$, i.e., $m^b \approx 1/t$. In two dimensions free bosons do not condense at finite temperature $T > 0$, however, the correlation length of the propagator $\langle \bar{b}_\nu b_{\nu'} \rangle$ grows exponentially for T below $T_{BE}^0 = 2\pi x/m^b \approx 2\pi xt$. In the x and T range we are interested in, $T \ll T_{BE}^0$, and the bosons can be considered almost condensed, i.e., $\bar{\Omega} \rightarrow 0$ and $\langle \bar{b}_\nu b_{\nu'} \rangle \approx \langle \bar{b}_\nu b_\nu \rangle = x$ for any ν, ν' .

III. PHASE DIAGRAM

The slave-boson mean-field theory has been put forward in numerous papers [48–52], originating in the Resonating Valence-Bond (RVB) idea [53]. In this section we review the phase diagram and briefly discuss some experimental implications in the superconducting phase at $T \rightarrow 0$. For simplicity a single CuO_2 -layer is considered, with $t = 2J$. Fig. 2 shows the phase diagram, derived from the numerical solution of Eqs. (19). It resembles those given in the literature [54,55], except at very small doping $x \rightarrow 0$, where our assumption of almost condensed bosons becomes incorrect. We also ignored the staggered-flux phase reported [56] for small x . These simplifications do not affect our results for the magnetic excitations.

Ignoring the lines labeled ‘AF’ for the moment, the phase diagram shows two transition temperatures T_d

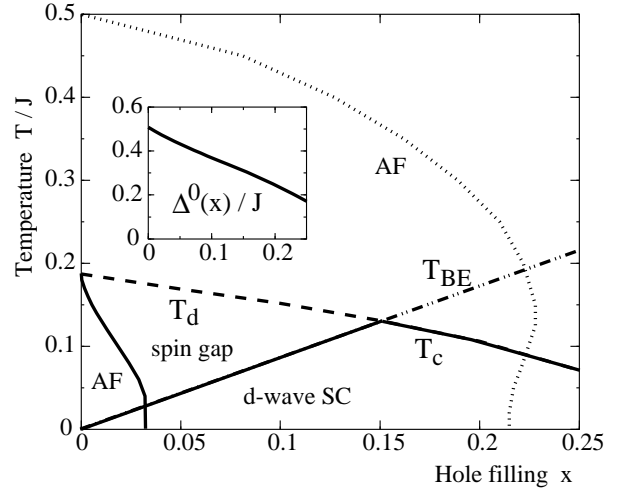


FIG. 2. **Main figure:** Mean-field phase diagram for a single CuO_2 -layer with $t = 2J$. T_d and T_{BE} denote transition temperatures to d-wave pairing of fermions and condensation of bosons, respectively. $T_c = \min\{T_d, T_{BE}\}$ is the physical T_c for bulk d-wave superconductivity. The lines labeled AF indicate the magnetic instability of the bare (dotted line) and renormalized theory (continuous), see text, Sec. IV. **Inset:** Maximum gap Δ^0 of fermions as function of hole filling at $T = 0$.

and T_{BE} . At temperatures $T > T_d$ the fermions move in the CuO_2 -plane with an effective dispersion $\varepsilon(\mathbf{k}) = -2\tilde{t}[\cos(k_x) + \cos(k_y)] - \mu^f$, where \tilde{t} in $\tilde{t} = xt + \frac{3}{8}J\tilde{\chi}$ is finite (uniform RVB phase). At $T = T_d$ they undergo a transition to the d-wave paired state with order parameter $\Delta(\mathbf{k}) = \frac{\Delta^0}{2}[\cos(k_x) - \cos(k_y)]$. This spin-gap phase is characterized by a gap $\Delta(\mathbf{k})$ for spin excitations, and is associated with the spin-gap (or pseudo-gap) regime observed in the normal state of underdoped cuprates. The bosons, on the other hand, show Bose condensation $\langle b_\nu \rangle \neq 0$ at $T = T_{BE}$. Bulk superconductivity is present for $T < T_c = \min\{T_d, T_{BE}\}$, where $\langle c_{\nu\uparrow} c_{\nu'\downarrow} \rangle = \langle b_\nu^\dagger \rangle \langle b_{\nu'}^\dagger \rangle \langle f_{\nu\uparrow} f_{\nu'\downarrow} \rangle \neq 0$. In two dimensions T_{BE} is identified with $T_{BE}^0 = 2\pi xt$, which yields a very large slope of the T_{BE} line in the phase diagram. Fluctuations of gauge fields around the mean-field solution are expected to reduce T_{BE}^0 to reasonable values [55]. The T_{BE} line sketched in Fig. 2 corresponds to that situation, with a maximum T_c at an optimal doping value $x_{opt} \approx 0.15$. The similarity of spin-gap and superconducting (SC) phase in mean-field theory naturally explains the persistence of the magnetic resonance into the spin-gap regime, although line-shape (damping) effects are missing.

In the following we focus on the SC state at $T \rightarrow 0$, which is reasonably reproduced by mean-field theory: In cuprate superconductors the underdoped region $x < x_{opt}$ shows unusual behavior of T_c , the superfluid density, and the maximum gap as function of hole filling. The superconducting T_c increases with doping, $T_c = T_{BE} \sim x$.

The superfluid density $\rho^s = n^s/m$ is given by the condensate density $\rho^b = n^b/m^b \sim x$ of bosons for small x , according to the Ioffe–Larkin formula [57]. Thus $\rho^s \sim x$, and the well known experimental observation [58] $\rho^s \sim T_c$ follows naturally. Tunneling and photoemission spectra are described by the Green’s function $G_{\nu\nu'}(\tau, \tau') = \langle \mathcal{T}_\tau \tilde{c}_{\nu\uparrow}(\tau) \tilde{c}_{\nu'\uparrow}^\dagger(\tau') \rangle$, where \tilde{c} is expressed by Eq. (2). In the superconducting state, where bosons are condensed in $\mathbf{k} = 0$, G splits into a coherent and incoherent part, $G = x \mathcal{G}^{ferm} + G^{incoh}$, where \mathcal{G}^{ferm} is the propagator of fermions. Thus the superconducting gap is given by the d-wave pairing gap of the fermions. Its doping dependence at $T = 0$ is shown in the inset of Fig. 2. When x is reduced from x_{opt} the maximum gap actually increases (whereas T_c decreases), as is seen in experiment [59–62]. At optimal doping mean-field theory gives $\Delta^0 \approx 0.3J \approx 40$ meV, which compares reasonably with experimental values [5]. On the overdoped side $x > x_{opt}$, $T_c = T_d$, and we get the BCS-like result $\Delta^0 \sim T_c$.

Recently an alternative slave-boson formulation has been proposed [63,64], which extends the SU(2) symmetry in particle–hole space of the 1/2-filled model [65] to the hole-doped case. Within mean-field theory the superconducting state at $T \rightarrow 0$ appears to be similar to the more conventional U(1) formulation we are using here, in particular is the magnetic spin-response the same.

IV. EFFECTIVE INTERACTION

So far we have not considered the possibility of antiferromagnetic (AF) order. It is known that wide areas of the mean-field phase diagram are unstable to AF order [66–69]. We determine the AF phase boundary from the diverging correlation length ξ_{AF} , which is extracted from the static ($\omega = 0$) susceptibility. For a single CuO₂-layer Eqs. (20)–(23) reduce to

$$\chi(\mathbf{q}, \omega) = \frac{\chi^{irr}(\mathbf{q}, \omega)}{1 + 2J[\cos(q_x) + \cos(q_y)] \chi^{irr}(\mathbf{q}, \omega)} \quad (24)$$

with χ in units [47] of $(g\mu_B)^2$. The irreducible part $\chi^{irr}(\mathbf{q}, \omega) = \chi_p^{irr}(\omega)$ is given by Eq. (23) with $p = (\mathbf{q}, p_z)$, $\tilde{p} = (\mathbf{k}, p_z)$ and arbitrary p_z . In Eq. (23), the internal summation is now over the 2D Brillouin zone, $\frac{1}{2N_L} \sum_{\tilde{p}} \rightarrow \frac{1}{N_L} \sum_{\mathbf{k}} = \int_{-\pi}^{\pi} d^2k / (2\pi)^2$, and dispersion and gap function become

$$\begin{aligned} \varepsilon &\equiv \varepsilon(\mathbf{k}) = T_p^f - \mu^f \text{ with } \tilde{t}^1 = 0; \quad \varepsilon' \equiv \varepsilon(\mathbf{k} + \mathbf{q}) \\ \Delta &\equiv \Delta(\mathbf{k}) = \Delta_{\tilde{p}} \text{ with } \Delta^{\perp 0} = 0; \quad \Delta' \equiv \Delta(\mathbf{k} + \mathbf{q}) \\ E &\equiv E(\mathbf{k}) = \sqrt{\varepsilon(\mathbf{k})^2 + \Delta(\mathbf{k})^2}; \quad E' \equiv E(\mathbf{k} + \mathbf{q}) \end{aligned} \quad (25)$$

Δ_p, T_p^f have been given in Eqs. (13,15,16). At the Néel wave-vector $\mathbf{Q} = (\pi, \pi)$ the static susceptibility takes the value $\chi_{AF} = \chi(\mathbf{Q}, 0)$, and for wave vectors \mathbf{q} close to \mathbf{Q} we get $J\chi(\mathbf{q}, 0) = 1 / [(\mathbf{q} - \mathbf{Q})^2 + \xi_{AF}^{-2}]$ with $\xi_{AF}^2 =$

$J\chi_{AF}$. Coming from high temperature or doping, an AF instability is indicated by $(\chi_{AF})^{-1} \rightarrow 0$. χ_{AF} has been calculated numerically, the resulting phase boundary is shown in Fig. 2 as a dotted line labeled ‘AF’. Our result is similar to the phase diagram obtained in Ref. [69].

Apparently, at zero temperature, AF order occurs at a quite high hole concentration $x_c^0 \approx 0.22$, which is totally inconsistent with experiment ($x_c \approx 0.02$). Furthermore, the study of magnetic properties in the paramagnetic phase is bound to $x > x_c^0$, i.e., the overdoped region. The high x_c^0 is an artifact of the mean-field approximation. Within the gauge-field approach it has been shown [70] that the AF ordered state at 1/2-filling $x = 0$ is quickly removed for $x > 0$. Furthermore it is known [66,71,72] that the interaction of spin-waves with doped holes destroys AF order at a small x_c . In order to treat underdoped systems we include these physics in a phenomenological fashion. We assume a renormalization of the magnetic interaction J_p in Eq. (20), such that x_c^0 is reduced to some $x_c \approx 0.03$. The model is to replace

$$J \rightarrow \alpha J, \quad \alpha = 0.35 \leftrightarrow x_c \approx 0.03 \quad (26)$$

in Eq. (21), J^\perp stays unchanged. The actual value of α is equivalent to choosing a specific critical doping x_c . As long as x_c is physically reasonable (≤ 0.05), results do not depend significantly on x_c . Using $J \rightarrow \alpha J$ in Eq. (24) we get a new AF phase boundary, which is shown in Fig. 2 as the continuous line ‘AF’.

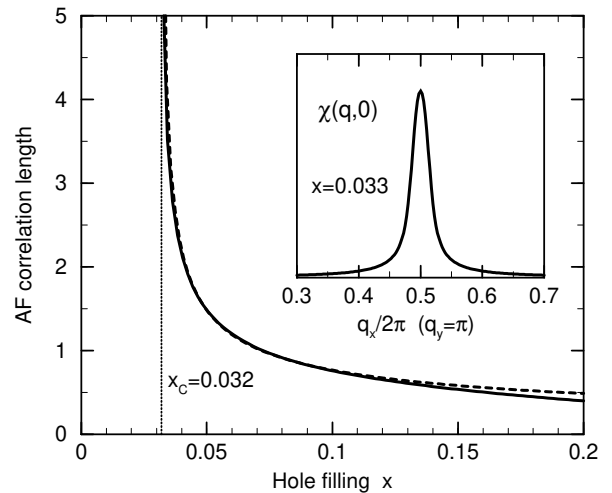


FIG. 3. **Main figure:** Antiferromagnetic (AF) correlation length ξ_{AF} at $T = 0$ in units of the lattice spacing. Continuous line: $\xi_{AF}(x)$ for an effective interaction $\alpha = 0.35$ (see text). The vertical dotted line indicates the AF instability at $x_c = 0.032$. Dashed line: Function $0.2/\sqrt{x - x_c}$, fitted to $\xi_{AF}(x)$ for $0.033 \leq x \leq 0.1$. **Inset:** Static susceptibility $\chi(\mathbf{q}, 0)$ (in arbitrary units) as a wave-vector scan over (π, π) in the 2D Brillouin zone, for $x = 0.033$ slightly above x_c . Shown is a scan in $(\pi, 0)$ -direction, scans in other directions look similar, indicating a commensurate AF transition. $\alpha = 0.35$ and $T = 0$ as above.

To give another argument in favor of the simple interaction model, especially the α being independent of doping, we consider the correlation length $\xi_{AF}(x)$ as function of hole filling. Fig. 3 shows ξ_{AF} , calculated with $J \rightarrow \alpha J$. It diverges at a $x_c = 0.032$ and decreases rapidly with additional doping, following $\xi_{AF}(x) \approx 0.2/\sqrt{x-x_c}$. This behavior is consistent with neutron-scattering measurements [73] on LSCO and results from high temperature series for the t - J -model [74]. The function $\sim 1/\sqrt{x}$ represents the average distance of doped holes and has been used in [73] to interpret the data. Finally it is noted that the AF transition at x_c occurs at the Néel wave vector $\mathbf{Q} = (\pi, \pi)$, i.e., is commensurate. This is shown in the inset of Fig. 3.

V. THE MAGNETIC RESONANCE

This section presents results for the magnetic response at the antiferromagnetic (AF) wave vector $\mathbf{Q} = (\pi, \pi)$. We consider a single CuO_2 -layer with a nearest and next-nearest neighbor hopping $t = 2J$ and $t' = -0.45t$, appropriate [75,46] for YBCO. Effects specific to the bi-layer structure of YBCO and BSSCO, namely the splitting of the magnetic response into acoustic and optical modes will be discussed separately in Section VII.

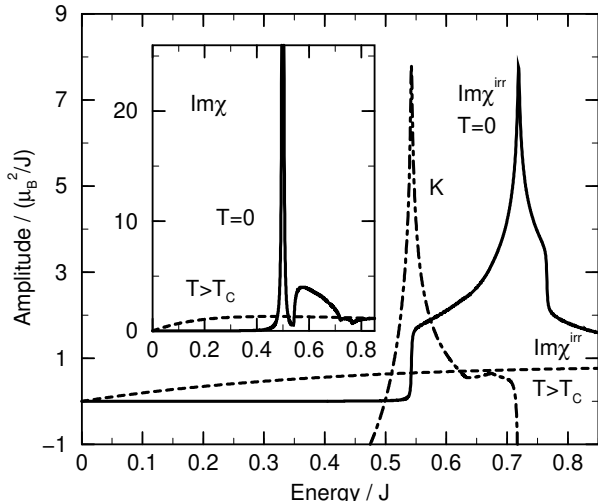


FIG. 4. Magnetic response at the AF wave vector (π, π) for a single CuO_2 -layer near optimal doping, $x = 0.12$. Parameters are $t = 2J$, $t' = -0.45t$. **Main figure:** Imaginary part of the bubble χ^{irr} in Eq. (24). Shown is the superconductor at $T = 0$ (cont. line) and the normal state $T = 0.2J > T_c$ (dashed line). The dashed-dotted line is the inverse Stoner-factor K (see text) for $T = 0$, scaled $\times(-5)$. **Inset:** Imaginary part of the resulting susceptibility χ , Eq. (24), for $T = 0$ (cont. line) and $T > T_c$ (dashed line). The sharp peak visible for $T = 0$ is actually a δ -function, broadened by a small damping used in the numerical calculation.

A. Results for the AF wave vector (π, π)

The dynamical susceptibility is obtained from Eq. (24) with the effective interaction $J \rightarrow \alpha J$, $\alpha = 0.35$ introduced in the preceding section. The integration in Eq. (23) is performed numerically on a 5000×5000 lattice in \mathbf{k} -space, with the infinitesimal $i0_+ \rightarrow i2\Gamma$ replaced by a small finite damping $2\Gamma = 0.001J$.

Calculations for a fixed hole filling $x = 0.12$ near optimal doping, based on mean-field parameters from the self-consistent solution of Eqs. (19) are shown in Fig. 4. In the superconducting (SC) state at $T = 0$ the imaginary part $\text{Im}\chi^{irr}(\mathbf{Q}, \omega)$ of the irreducible bubble is characterized by a gap up to a threshold energy $\Omega_0 \approx 0.54J$, with a step-like van Hove singularity (v.H.s.) at the onset of spectral weight at $\omega = \Omega_0$. A peak at $\omega \approx 2\Delta^0 = 0.72J$ is remnant of the density of states of the d-wave superconductor. The corresponding real part is shown in Fig. 4 as the inverse Stoner-enhancement factor $K(\mathbf{Q}, \omega) = [1 - \alpha 4J \text{Re}\chi^{irr}(\mathbf{Q}, \omega)]$. By virtue of the Kramers-Kronig transformation, the step at the threshold Ω_0 in $\text{Im}\chi^{irr}$ turns into a log-singularity in $\text{Re}\chi^{irr}$, and $K(\mathbf{Q}, \omega)$ crosses zero at an energy $\omega_{res} = 0.5J < \Omega_0$ within the gap. This leads to an undamped δ -like resonance at ω_{res} in the magnetic response $\text{Im}\chi(\mathbf{Q}, \omega)$, as is shown in the inset of Fig. 4. The position $\omega_{res} = 0.5J \approx 60$ meV is not too far off the ≈ 40 meV observed in optimally doped YBCO and BSSCO. The situation changes drastically in going to the normal state $T > T_c \approx T_d$. As is seen from the dashed line in Fig. 4 (main figure), $\text{Im}\chi^{irr}(\mathbf{Q}, \omega)$ loses its structure, in particular the gap vanishes. The corresponding K (not shown in the figure) becomes equally structure-less without any zero crossing, leading to a vanishing of the resonance in $\text{Im}\chi$ in the normal state (inset of Fig. 4).

The effect of underdoping is demonstrated in Fig. 5. For comparison with experiment $\text{Im}\chi$ in the inset has been broadened to an experimental resolution (FWHM) of $4\Gamma \approx 5$ meV through a damping $i0_+ \rightarrow 2\Gamma = 0.02J$ in Eq. (23). When x is reduced from $x = 0.12$ the gap Ω_0 in $\text{Im}\chi^{irr}$ decreases monotonously, and with it the resonance at $\omega_{res} \lesssim \Omega_0$ moves to lower energies. ω_{res} reaches zero at the AF transition, which occurs at $x_c = 0.023$ for the parameters used here (x_c depends slightly on t' , since $\alpha = 0.35$ is held fixed). Note that ω_{res} moves opposite to the maximum gap Δ^0 . The latter increases when x decreases (see Fig. 2) and is reflected in the peak in $\text{Im}\chi^{irr}$ at higher energies $\omega = 2\Delta^0 = 0.72 \dots 0.80$ in Fig. 5. The spectral weight $W = \int d\omega \text{Im}\chi$ increases [76] when x is reduced, since the system is shifted closer to the magnetic instability. For a quantitative comparison of W we follow a procedure applied to experimental INS data in Ref. [76,8]. For $x = 0.12$ the flat normal-state spectrum is subtracted as a background from the $T = 0$

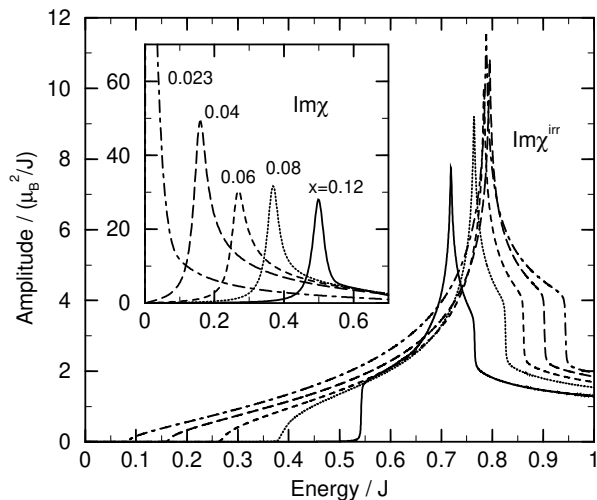


FIG. 5. Magnetic response at wave vector (π, π) as in Fig. 4, for optimal to underdoped hole filling in the superconducting state $T = 0$. **Main figure:** Imaginary part of χ^{irr} . Curves are identified by the respective onset of spectral weight (threshold), which is $0.54J$ for $x = 0.12$ and decreases for $x = 0.08, 0.06, 0.04, 0.023$ down to $0.09J$. **Inset:** Imag. part of the susceptibility χ . Here the peaks are broadened to an experimental resolution (FWHM) of $4\Gamma \approx 5$ meV.

curve shown in Fig. 5, inset. Integrating only the positive part of the resulting difference spectrum gives the weight ΔW of the resonance compared to the normal state. We find $\Delta W = 1.55 \mu_B^2$, which agrees well with optimally doped YBCO. With reducing x the resonance also develops some intrinsic damping. The step-height at the threshold Ω_0 in $\text{Im}\chi^{irr}$, which is responsible for the δ -like resonance, decreases and eventually vanishes around $x = 0.09$.

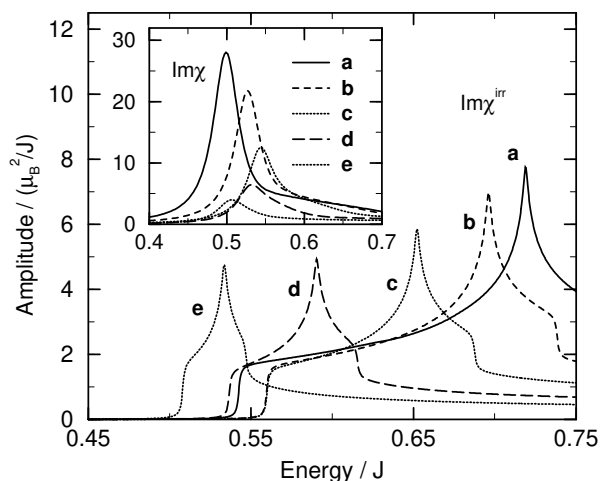


FIG. 6. Magnetic response at $\mathbf{q} = (\pi, \pi)$ for optimal to overdoping at $T = 0$. Parameters as in Fig. 5, except hole filling. **Main figure:** Bubble spectrum $\text{Im}\chi^{irr}$ for $x = 0.12$ (curve a), 0.14 (b), 0.18 (c), 0.24 (d), 0.30 (e). **Inset:** Corresponding $\text{Im}\chi$, broadened to $4\Gamma \approx 5$ meV.

The effect of overdoping is presented in Fig. 6. When x is increased from 0.12 up to 0.3, the ph-threshold Ω_0 in $\text{Im}\chi^{irr}$ and with it the position of the resonance first grows, but ω_{res} starts to decrease around $x = 0.18$. This trend is consistent with recent INS experiments [11] on overdoped BSCCO, where the resonance appeared at an energy ω_{res} reduced from the optimally doped case [10].

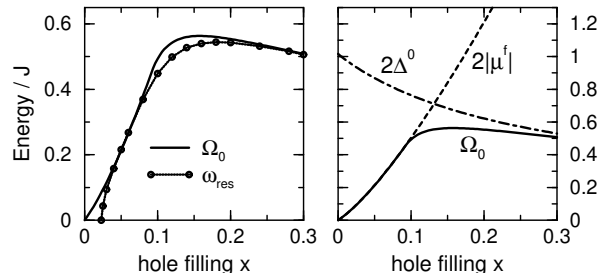


FIG. 7. **Left panel:** Particle-hole excitation threshold Ω_0 and resonance position ω_{res} as function of hole filling in the SC state. Ω_0 is given by Eq. (27), and ω_{res} is the energy of the peak maximum in $\text{Im}\chi$, extracted from plots like Figs. 5, 6 (insets). **Right panel:** Comparison of Ω_0 , the chemical potential $\mu^f = -|\mu^f|$ of fermions, and the maximum gap Δ^0 .

Fig. 7 (left) summarizes the doping dependence of the resonance. ω_{res} is always located slightly below the threshold Ω_0 to the damping particle-hole continuum. Near the magnetic instability [77] at $x = x_c = 0.023$ and around optimal doping $x \approx 0.1 \dots 0.2$, the resonance is a δ -function, well separated from the continuum. The x -dependent threshold is given by

$$\Omega_0 = \begin{cases} 2|\mu^f| \sqrt{\sigma(2-\sigma)} & \text{for } \sigma < 1 \\ 2|\mu^f| & \text{for } \sigma \geq 1 \end{cases} \quad (27)$$

with $\sigma = (\Delta^0)^2 / 8xt'\mu^f$. For $x < \bar{x} \approx 0.09$ it is $\sigma > 1$ and therefore $\Omega_0 = 2|\mu^f|$. That is, in the underdoped regime the resonance energy follows the chemical potential $|\mu^f| = -\mu^f$ of the fermions, and thus increases with hole filling. The gap Δ^0 , on the contrary, decreases. This is illustrated in the right panel of Fig. 7. Around $x = 0.13$, where $|\mu^f| = \Delta^0$, a crossover into the overdoped regime occurs, where $\Omega_0 \approx 2\Delta^0$ for large x . The increase of ω_{res} turns into a decrease. Compared to experiment [11] the latter is too weak; this is due to Δ^0 (and $T_c = T_d$) decreasing too slowly with x in the self-consistent mean-field calculation.

It has been pointed out above that the resonance depends on the d-wave gap to be present, i.e., the superconducting or spin-gap state, and a sufficient next-nearest neighbor hopping $t' < 0$. The influence of t' becomes apparent, if the bubble χ^{irr} and the resulting magnetic spectrum $\text{Im}\chi$ at $T = 0$ are re-calculated for $t' = 0$ (not shown in the figures). The response $\text{Im}\chi$ no longer contains a resonance-like peak, although the spectral weight is conserved. Only for small $x \rightarrow x_c$ at the magnetic

instability $\text{Im}\chi$ develops a Goldstone (Bragg) peak. The bubble spectrum at the threshold $\Omega_0 = 2|\mu^f|$ now follows $\text{Im}\chi^{irr}(\mathbf{Q}, \omega) \sim \sqrt{\omega - \Omega_0}\Theta(\omega - \Omega_0)$ for the whole range of x , and a step-like v.H.s. never appears.

B. Discussion

The results presented above compare well to neutron-scattering experiments [8,9]: The variation of the resonance energy ω_{res} with hole filling x is reproduced in the underdoped [6,7,76,12] and the overdoped [4,10,11] regime. At optimal doping the resonance appears resolution limited (as a delta function) in the SC state only [2,3], and its energy and spectral weight are comparable to the values measured in experiment [8]. In the underdoped regime it is obtained also in the spin-gap phase [6,7,12] above T_c ; the observed line-shape (damping) is not reproduced in mean-field theory. YBCO and BSCCO are bi-layer materials, i.e., consist of two coupled CuO_2 planes per unit cell. However, for the resonance to emerge the bi-layer structure is not important. Rather, in optimally and slightly underdoped systems it depends on a hole-like Fermi surface (i.e., a sufficient $t' < 0$) and a finite d-wave (spin-) gap. As will become clear in Section VII this conclusion is not altered if the double-layer structure is taken into account.

The slave-particle approach reproduces quite satisfactorily the resonance energy ω_{res} in the underdoped regime, where ω_{res} is *not* connected to the maximum gap Δ^0 , see Fig. 7. ω_{res} is given by the pole of Eq. (24), i.e., the energy of the bound state in the particle-hole channel of the fermions. In the underdoped regime $\omega_{res} \lesssim 2|\mu^f|$ follows the chemical potential $|\mu^f| = -\mu^f$. μ^f refers to quasi particles (the fermions) which emerge from the mean-field description of the t - J -model and are strongly renormalized. They propagate with hopping matrix-elements $\tilde{t} = xt + \frac{3}{8}J\tilde{\chi} \approx xt + 0.15J$, $\tilde{t}' = xt'$, and hence Fermi velocity $\tilde{v}_F \approx xv_F$, that are reduced from the bare parameters by the small Gutzwiller factor $x \leq 0.15$. The latter mimics the reduced phase space due to local correlations in the doped Mott insulator. Accordingly $|\mu^f|$ comes out small enough, such that in the underdoped regime $|\mu^f| < \Delta^0$, and $\omega_{res} \lesssim 2|\mu^f|$ is determined by $|\mu^f|$, which increases with hole filling x . In contrast, if unrenormalized quasi particles (QP) are assumed with bare t, t', v_F , the chemical potential $|\mu| \sim \frac{1}{x}|\mu^f| \gg \Delta^0$, and $\omega_{res} \lesssim 2\Delta^0$ is connected to the gap for almost all x , which decreases with x . To achieve a satisfactory result from unrenormalized QP the effective (residual) interaction [78] has to be made doping dependent. This is the case in theories based on the spin-fermion model [27,28], where the coupling constant is controlled by a magnetic correlation length, which can be chosen x -dependent.

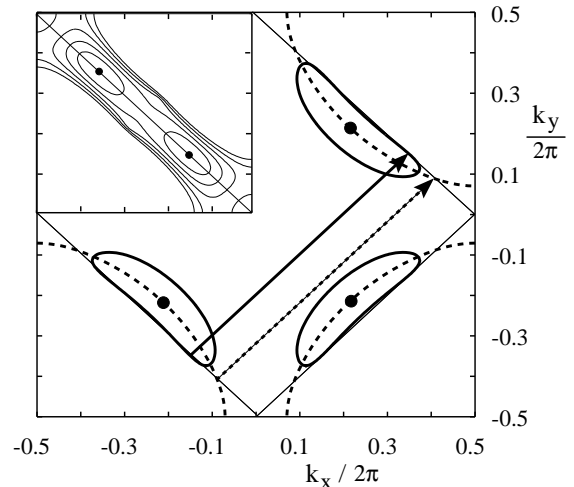


FIG. 8. Origin of the threshold for particle-hole (ph) excitations with wave vector (π, π) , corresponding to the spectra in Fig. 4. **Main figure:** 2D Brillouin zone (BZ) with the underlying normal-state Fermi surface (FS) for $t = 2J, t' = -0.45t$ as dashed lines. The dashed arrow indicates a ph-excitation with $\mathbf{q} = (\pi, \pi)$ at a minimal energy $\Omega_0 = 0$. In the superconducting state the FS collapses to nodes (indicated as dots), and $\Omega_0 > 0$. The full arrow connects two constant-energy lines of quasi-particles $E(\mathbf{k}) = \Omega_0/2$. **Inset:** ph-excitation energies $\Omega(\mathbf{q}, \mathbf{k})$ of the superconductor for $\mathbf{q} = (\pi, \pi)$ in the upper right BZ/4. Shown are the minima Ω_0 as dots and the first 5 higher energies as lines. Line distance is $0.05J$.

C. Properties of the ph-threshold Ω_0

In the remainder of this section we study in some detail the origin and qualitative properties of the threshold Ω_0 in the bubble spectrum $\text{Im}\chi^{irr}(\mathbf{q}, \omega)$ at $\mathbf{q} = (\pi, \pi)$. The presence of this threshold and the step-like onset of spectral weight at $\omega = \Omega_0$ in the superconducting state lead to the sharp resonance. We consider $\text{Im}\chi^{irr}$ at $T = 0$, which reads from Eq. (23) with (25) for $\omega > 0$

$$\text{Im}\chi^{irr}(\mathbf{q}, \omega) \sim \sum_{\mathbf{k}} \delta(\omega - \Omega(\mathbf{q}, \mathbf{k})). \quad (28)$$

BCS coherence factors have been ignored. It is determined by the particle-hole (ph) excitation energies $\Omega(\mathbf{q}, \mathbf{k}) = E(\mathbf{k}) + E(\mathbf{k} + \mathbf{q})$ of fermions. The pair momentum \mathbf{q} is set to $\mathbf{Q} \equiv (\pi, \pi)$ in the following. Fig. 8 illustrates the situation for $x = 0.12$ near optimal doping, corresponding to the spectra shown in Fig. 4. In the normal state $T > T_c$ a ph-excitation connects two points of the underlying Fermi surface (FS), and the threshold $\Omega_0 = \min_{\mathbf{k}} \Omega(\mathbf{Q}, \mathbf{k})$ is 0. In the superconducting state a finite Ω_0 is at first sight surprising, since the d-wave SC has a finite density of states. However, when the FS collapses to nodes, a minimum energy $\Omega_0 > 0$ has to be paid for ph-excitations with wave-vector \mathbf{Q} . It turns out that $\Omega(\mathbf{Q}, \mathbf{k})$ is minimal, if $E(\mathbf{k}) = E(\mathbf{k} + \mathbf{Q}) = \Omega_0/2$,

with the lines of constant energy $E(\mathbf{k}) = \Omega_0/2$ touching the reduced (magnetic) Brillouin zone at 8 points. These points are connected by \mathbf{Q} as indicated by the full arrow in Fig. 8. Apparently $E(\mathbf{k}) = \Omega_0/2$ is very flat near these points, close to a (dynamic) nesting condition. This is due to the bandstructure of the underlying normal state, in particular the $t' < 0$, and the presence of the d-wave gap $\Delta(\mathbf{k})$. The resulting ph-dispersion $\Omega(\mathbf{Q}, \mathbf{k})$ is shown in the inset of Fig. 8. It displays two minima per 1/4 Brillouin zone with energy $\Omega(\mathbf{Q}, \mathbf{k}^0) = \Omega_0$, which fall on the line $k_x^0 + k_y^0 = \pi$. The neighborhood of these minima is quite flat, and Ω can be expanded as $\Omega(\mathbf{Q}, \mathbf{k}) \approx \Omega_0 + a_1(k_1)^2 + a_2(k_2)^2$, with $k_{1,2} = \frac{1}{\sqrt{2}}((k_x - k_x^0) \pm (k_y - k_y^0))$ and relatively small $a_1, a_2 > 0$. Eq. (28) then shows a step-like van Hove singularity (v.H.s.) at Ω_0 , $\text{Im}\chi^{irr}(\mathbf{Q}, \omega) \sim \Theta(\omega - \Omega_0) / \sqrt{a_1 a_2}$. The value of Ω_0 is given by Eq. (27) with $\sigma < 1$.

When the hole filling x is reduced, the two minima in $\Omega(\mathbf{Q}, \mathbf{k})$ move closer, until they merge at $k_x^0 = k_y^0 = \pi/2$ for $x = \bar{x} \approx 0.09$, which corresponds to $\sigma = 1$ in Eq. (27). The step-v.H.s. vanishes on the course (see Fig. 5), since $\Omega(\mathbf{Q}, \mathbf{k})$ becomes increasingly steep in k_1 direction. For $x < \bar{x}$ we have $\sigma > 1$, and $\text{Im}\chi^{irr}$ may be approximated by setting $t' = 0$, leading to [79] $\text{Im}\chi^{irr}(\mathbf{Q}, \omega) \sim \sqrt{\omega - \Omega_0} \Theta(\omega - \Omega_0)$. I.e., the step at the threshold Ω_0 has changed into a $\sqrt{\omega}$ behavior.

VI. INCOMMENSURATE RESPONSE

The resonance at $\omega_{res} = 40$ meV, as well as its relative in underdoped samples with reduced $\omega_{res} < 40$ meV is characterized as a single (commensurate) peak at $\mathbf{q} = (\pi, \pi)$ in wave-vector space [2–4,7]. Above the resonance energy an incommensurate structure has been observed [34,36,37], with broad maxima following a dispersion similar to spin waves. Recently, inelastic neutron-scattering (INS) experiments on underdoped [9,35,36,80] and optimally [9,37,81] doped YBCO revealed that also the magnetic response below the resonance position shows incommensuration: Four distinct peaks appear at $\mathbf{q} = (\pi \pm \delta, \pi)$ and $(\pi, \pi \pm \delta)$, which move away from (π, π) with decreasing energy, i.e., are described by some ‘upside-down’ dispersion [36,37]. The incommensurability is of “parallel” type, peaks are displaced in $(\pi, 0)$ and $(0, \pi)$ -direction from (π, π) , similar to those observed [39,40] in LSCO. This is not expected in a d-wave BCS picture [14,82], since at low energies the particle-hole excitations from node to node should dominate, leading to four peaks at $\mathbf{q} = (\pi \pm \delta', \pi \pm \delta')$. In this section we demonstrate that a parallel incommensurability actually occurs in a range of energies below the resonance.

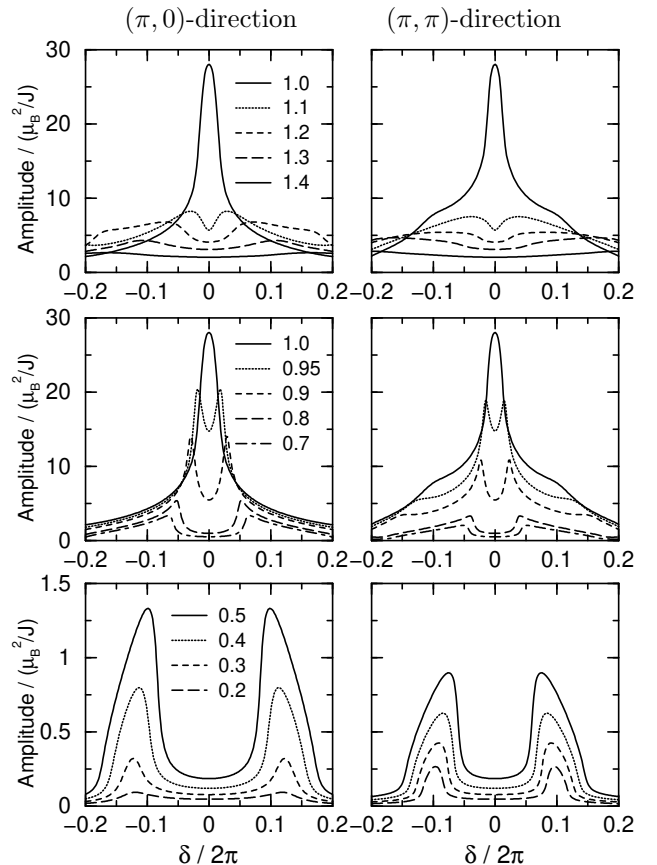


FIG. 9. Wave-vector \mathbf{q} scans of $\text{Im}\chi(\mathbf{q}, \omega)$ at fixed energy ω , for $t = 2J, t' = -0.45t, x = 0.12$ in the superconducting state at $T = 0$. A quasi-particle damping $\Gamma = 0.01J$, corresponding to an experimental energy resolution (FWHM) of $4\Gamma \approx 5$ meV has been used. \mathbf{q} is measured from (π, π) : $\delta_{x,y} = q_{x,y} - \pi$, $\delta = \pm\sqrt{\delta_x^2 + \delta_y^2}$. **Left column:** Scans in $(\pi, 0)$ -direction, i.e., $\delta_y = 0$. **Right column:** (π, π) -direction, $\delta_y = \delta_x$. **Top row:** Sequence of energies $\omega/\omega_{res} = 1.0 \dots 1.4$ at and above the resonance energy $\omega_{res} = 0.5J$. **Middle row:** $\omega/\omega_{res} = 1.0 \dots 0.7$ at and below ω_{res} . **Bottom row:** Energies far below ω_{res} , showing a crossover from parallel to diagonal incommensurability. Note the different vertical scale.

A. Structure of the magnetic response in wave-vector space

Fig. 9 presents wave-vector scans of the magnetic susceptibility $\text{Im}\chi(\mathbf{q}, \omega)$ for YBCO in the superconducting state at $T = 0$. For comparison with INS data an experimental energy resolution $4\Gamma \approx 5$ meV has been simulated through a quasi-particle damping $\Gamma = 0.01J$. For $\omega = \omega_{res}$ scans in parallel $(\pi, 0)$ as well as diagonal (π, π) -direction show a commensurate sharp peak. When energy is increased (top panel), the resonance first evolves into a broad incommensurate structure with maxima dispersing like spin waves [8,36]. At higher energies around $2\Delta_0 \approx 1.5\omega_{res}$ this turns into some featureless background. When the energy is reduced from ω_{res}

(middle panel), the peak also splits in parallel as well as diagonal direction, suggesting a circular structure in \mathbf{q} -space. However, the maximum intensity is higher in $(\pi, 0)$ -direction, reproducing the experimental observation. The case $\omega/\omega_{res} \approx 0.7$ can be compared to a study [35] on underdoped $\text{YBa}_2\text{Cu}_3\text{O}_{6.6}$: The ratio of max. intensities $I_{par}/I_{diag} \approx 1.7$ from Fig. 9 is consistent to the $\lesssim 2.0$ we read off the INS data in Ref. [35]. The range $\delta = \delta_x = 0.052 \dots 0.065$ of the displacement of peaks in $(\pi, 0)$ -direction is comparable to experimental values [83] reported [35,37] for the same range of energies $\omega/\omega_{res} = 0.8 \dots 0.7$. In the bottom panel, where the energy is reduced even further, I_{par} starts to weaken relative to I_{diag} . For $\omega/\omega_{res} < 0.35$ the peaks in the diagonal (π, π) -direction eventually dominate, as is expected from a d-wave superconductor in mean-field theory at $\omega \rightarrow 0$. However, such a crossover from parallel to diagonal incommensurability at low ω is not observed in experiment. At low energies the INS data indicate a strong isotropic suppression [9,37], similar to what is seen [40,84] in LSCO.

In the normal state, INS on the optimally doped compound shows a broad commensurate peak, its width depending weakly on energy [37]. From the calculation at $T > T_c \approx T_d$ we get indeed a response almost independent of wave vector and energy, as is expected from the absence of nesting properties of the underlying Fermi surface (see Fig. 8). Note that both the commensurate (at ω_{res}) and incommensurate intensity vanish in the normal state, as is observed [37] in INS. The situation is different in underdoped YBCO, where the spin-gap regime is entered as $T > T_c$. In mean-field theory the spin-gap phase is similar to the SC, with the SC gap becoming the spin gap (see Section III). Therefore the pattern in the magnetic response at $\omega \leq \omega_{res}$ persists at $T > T_c$, which has also been observed in underdoped systems [36,80]. Experimental line shapes at $T > T_c$ are not reproduced in mean-field; however, we expect significant damping in the spin-gap phase if fluctuations are included.

B. The dynamic nesting effect

An explanation of the incommensurate pattern below ω_{res} in the superconducting state can be found in the dispersion $E(\mathbf{k})$ of the Gutzwiller-renormalized fermions [42]. At vanishing energy $\omega \rightarrow 0$ only particle-hole (ph) excitations $\Omega(\mathbf{q}, \mathbf{k})$ with \mathbf{q} connecting two d-wave nodes $E(\mathbf{k}) \gtrsim 0$, $E(\mathbf{k} + \mathbf{q}) \gtrsim 0$ are possible. At finite hole doping the nodes are shifted from $(\pm\pi/2, \pm\pi/2)$ towards the Γ -point $(0, 0)$; thus the bubble spectrum $\text{Im}\chi^{irr}$ features peaks [82] at $\mathbf{q} = (\pi \pm \delta', \pi \pm \delta')$, diagonally displaced from (π, π) . The curves for low $\omega/\omega_{res} = 0.2, 0.3$ in Fig. 9 are still dominated by this type of ph-excitation. With increasing energy a different process gains importance, where \mathbf{q} connects two contours $E(\mathbf{k}) = \omega/2$ in the Brillouin zone.

Each d-wave node is surrounded by such a ‘banana-shaped’ contour, and in an energy range around $\omega_{inc} \approx 0.7\omega_{res}$, where the parallel incommensurate pattern in $\text{Im}\chi(\mathbf{q}, \omega_{inc})$ is most pronounced, these $E(\mathbf{k})$ show almost flat pieces parallel to the magnetic zone boundary. This gives rise to a dynamic nesting contribution [85,86], which favors peaks at $\mathbf{q} = (\pi \pm \delta, \pi), (\pi, \pi \pm \delta)$. In particular, at $\omega = \omega_{inc}$ a ratio of intensities $I_{par}/I_{diag} \lesssim 2$ is expected from the nesting argument, which is close to the value drawn from the numerical calculation (Fig. 9) as well as experiment. An illustration of this effect has been given in Ref. [42] in Fig. 5.

In the preceding section it became apparent that the commensurate resonance at (π, π) depends on a sufficiently large n.n.n. hopping $t' < 0$. With respect to the (parallel) incommensurate pattern this is not the case: The underlying dynamic nesting effect is a general feature of the d-wave superconductor. This is confirmed in a calculation of \mathbf{q} -scans for $t' = 0$: The parallel incommensurability dominates for energies above the crossover from the diagonal one and below $\approx 2|\mu^f|$, where $\text{Im}\chi$ becomes broad and commensurate.

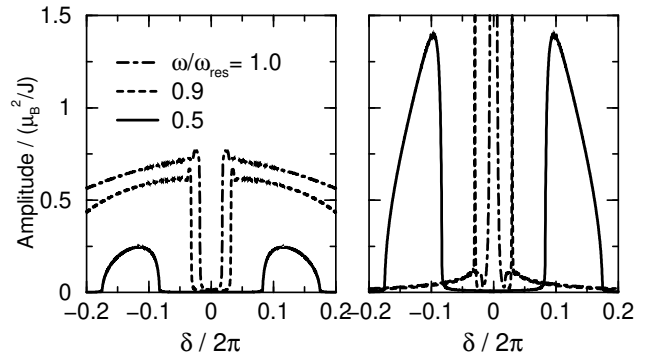


FIG. 10. Wave-vector scans in $(\pi, 0)$ -direction as in Fig. 9, left column, but with $4\Gamma = 0.002J$. Shown are $\omega/\omega_{res} = 1.0, 0.9, 0.5$. **Left:** Bubble spectrum $\text{Im}\chi^{irr}$. **Right:** Magn. response $\text{Im}\chi$. The curves for 1.0 and 0.9 are scaled $\times 0.01$; the one for 1.0 features a δ -type peak, see text.

C. Dispersion of the resonance

Returning to the case $t' = -0.45t$, for energies increasing towards the resonance energy ω_{res} the incommensurate pattern eventually merges into the commensurate resonance, as is seen in Fig. 9, middle row. This is due to the final-state interaction Eq. (24), which develops a pole at the commensurate position (π, π) for $\omega = \omega_{res}$. In Fig. 10 scans similar to Fig. 9 are made in $(\pi, 0)$ -direction, with the ‘experimental damping’ omitted. For $\omega/\omega_{res} = 0.5$ the bubble spectrum $\text{Im}\chi^{irr}(\mathbf{q}, \omega)$ features two humps in $(\pi, 0)$ -direction, and is zero outside these regions (left panel). This is due to a \mathbf{q} -dependent

threshold $\Omega_0(\mathbf{q}) = \min_{\mathbf{k}} \Omega(\mathbf{q}, \mathbf{k})$. With the interaction αJ switched on, $\chi^{irr} \rightarrow \chi$, the humps are merely amplified in intensity (right panel), and the nesting argument can be applied as above. When ω is increased, the two humps move closer. Additionally, sharp peaks appear in $\text{Im}\chi$, which eventually merge in a single δ -like resonance at (π, π) for $\omega \rightarrow \omega_{res}$. The incommensurate structure still present in the bubble spectrum for $\omega/\omega_{res} = 1.0$ is completely superseded by the pole of Eq. (24). The latter is driven by the bubble's real part $\text{Re}\chi^{irr}$, which at $\omega = \omega_{res}$ is strongly peaked at (π, π) in \mathbf{q} -space, assisted by the interaction $J(\mathbf{q}) = J[\cos(q_x) + \cos(q_y)]$, which also favors the wave vector (π, π) .

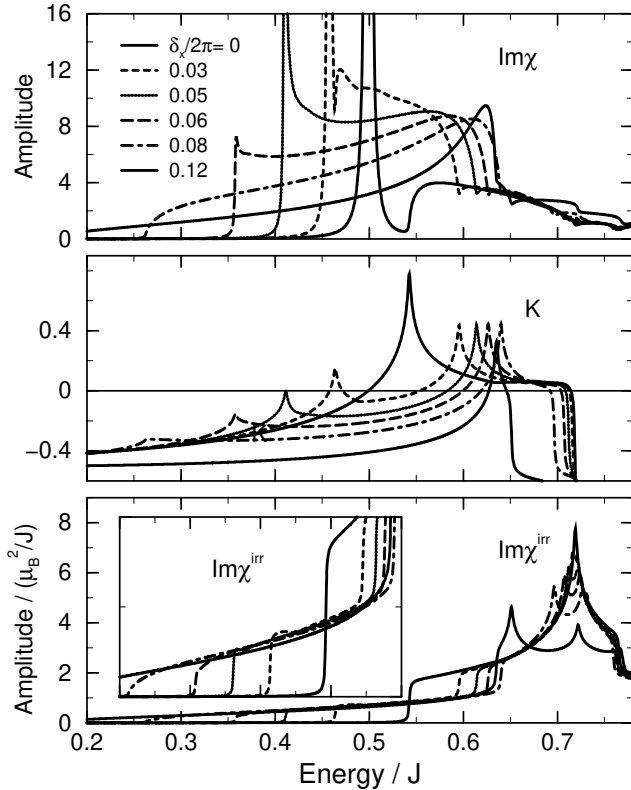


FIG. 11. Dispersion in $(\pi, 0)$ -direction for $x = 0.12$. Parameters as in Fig. 4. Shown is a sequence of wave vectors $\delta_x = (0 \dots 0.12) 2\pi$, $\delta_y = 0$. **Bottom panel:** Bubble spectrum $\text{Im}\chi^{irr}$; **Inset:** Zoom of the threshold region. **Middle:** Inverse Stoner factor $K \times (-1)$. **Top:** Resulting response $\text{Im}\chi$ from RPA.

It is instructive to look at the commensurate–incommensurate crossover also in energy space, using the ω -scans in Fig. 11 for several fixed wave vectors $\delta_x = q_x - \pi$, $q_y = \pi$. At $\mathbf{q} = (\pi, \pi)$ the bubble spectrum $\text{Im}\chi^{irr}(\mathbf{q}, \omega)$ features a single step-like onset of spectral weight at the particle–hole (ph) excitation threshold Ω_0 ; its consequences for the formation of the neutron resonance have been discussed in Section V above. In Fig. 11 (bottom) it is demonstrated how this threshold splits into two structures as we move

away from (π, π) : the ph-threshold $\Omega_0(\mathbf{q})$ itself, shifting to lower energies, and a second step-like onset of additional spectral weight at some $\Omega_2(\mathbf{q}) \geq \Omega_0(\mathbf{q})$, which shifts up with δ_x . The denominator (real part) of Eq. (24), $K(\mathbf{q}, \omega) = [1 + \alpha 2J[\cos(q_x) + \cos(q_y)]\text{Re}\chi^{irr}(\mathbf{q}, \omega)]$ thus shows a splitting of the corresponding log singularity into two (middle panel in Fig. 11), which in turn produces two peaks in the magnetic response $\text{Im}\chi(\mathbf{q}, \omega)$ (top panel). One of these peaks disperses to lower energies and is identified as the \mathbf{q} -dependent resonance, since it is located below the threshold $\Omega_0(\mathbf{q})$ and is therefore sharp. With increasing δ_x its spectral weight is continuously reduced, since the height of the step at $\Omega_0(\mathbf{q})$ in $\text{Im}\chi^{irr}$ decreases. The other peak near $\Omega_2(\mathbf{q})$ disperses to higher energies. It appears merely as a broad peak or shoulder within the damping continuum. It is responsible for the spin-wave like dispersion of broad maxima above ω_{res} in Fig. 9 (top). The resonance, on the other hand, follows an upside-down dispersion and produces the incommensurate peaks below ω_{res} in Fig. 9 (middle row).

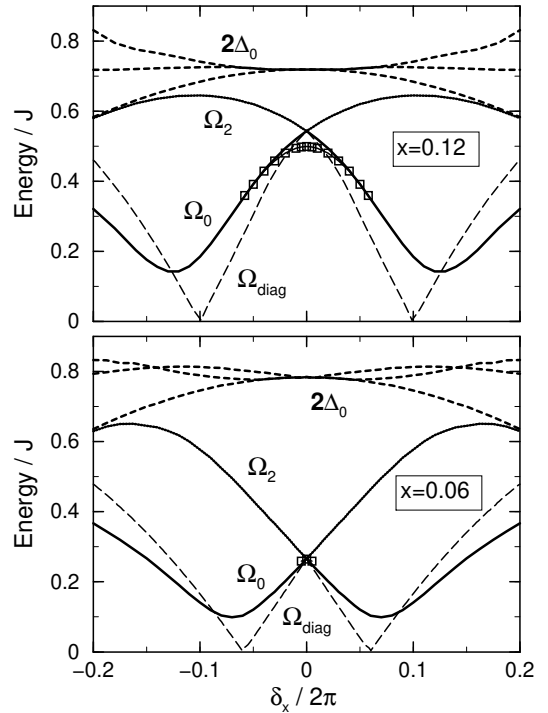


FIG. 12. Dispersion of features of the bubble spectrum $\text{Im}\chi^{irr}$ and the spin-1 bound state (resonance) in $\text{Im}\chi$. $\delta_x = (q_x - \pi)$, $q_y = \pi$. Shown is the ph-threshold Ω_0 , the 2nd onset of weight Ω_2 , and the three v.H.s. associated with $2\Delta_0$. The position ω_{res} of the resonance is indicated by squares. The ph-threshold Ω_0 is also given in (π, π) -direction as Ω_{diag} .

Results for the $(\pi, 0)$ -direction and doping level $x = 0.12$ are summarized in Fig. 12 (top). It displays the ph-threshold $\Omega_0(\mathbf{q})$, the second onset of spectral weight $\Omega_2(\mathbf{q})$, and the resonance position $\omega_{res}(\mathbf{q})$ where it exists. For comparison the ph-threshold $\Omega_{diag}(\mathbf{q})$ in (π, π) -

direction is also shown. In contrary to $\Omega_0(\mathbf{q})$ it has zeroes at $\delta_x = \pm(\sqrt{2}k_F - \pi)$, where \mathbf{q} connects two d-wave nodes. In addition the energies of the van Hove singularities (v.H.s.) associated with $2\Delta_0$ are given in the figure. At $\mathbf{q} = (\pi, \pi)$ the bubble spectrum $\text{Im}\chi^{irr}$ (Fig. 4) shows a single v.H.s. at $\omega = 2\Delta^0 \approx 0.72J$. From Fig. 11 (bottom) it can be seen that this v.H.s. splits into three peaks with quite flat dispersion.

The effect of strong underdoping is demonstrated in the bottom panel of Fig. 12 for $x = 0.06$: The ph-threshold Ω_0 at $\mathbf{q} = (\pi, \pi)$ and with it the resonance position shift down (compare also Fig. 7). The \mathbf{q} -range, where a sharp resonance exists, shrinks [87], and the upside-down dispersion narrows. On the other hand, the v.H.s. around $2\Delta_0$ as well as the maximum of Ω_2 vary only weakly with doping (Δ_0 increases slightly with underdoping). This will become important in the calculation of wave-vector integrated susceptibilities in Section VII below.

D. Discussion

The parallel type of incommensurability, i.e., a maximum intensity at the points $\mathbf{q} = (\pi, \pi \pm \delta)$, $(\pi \pm \delta, \pi)$ in the Brillouin zone is a generic feature of the d-wave SC state. In an energy range below $2\Delta^0$ the intensity is enhanced at these points due to the dynamic nesting mechanism [42]. At very low energies, on the other hand, excitations from node to node in (π, π) direction dominate [82] and lead to a crossover to the diagonal type as $\omega \rightarrow 0$. It should be noted that the parallel incommensurability is not related to ‘‘stripes’’ [88–90], i.e., we do not consider the possibility of a combined ordering of charge and spin into quasi one-dimensional structures. Incommensurate pattern in $\text{Im}\chi(\mathbf{q}, \omega)$ and their dispersion have been obtained with similar slave-particle methods [15,91,92], BCS theory [22,23,93], or the FLEX approximation for the Hubbard model [26,94]. The present slave-particle approach predicts how the dispersion of the resonance (associated with $\Omega_0(\mathbf{q})$ in Fig. 12) and the spin-wave like dispersion of broad peaks above it (following $\approx \Omega_2(\mathbf{q})$) change with underdoping. When x is reduced, the peaks connected to $\Omega_2(\mathbf{q})$ should be observable in a wider energy range above the resonance. Furthermore, near the bottom of Ω_2 at $\mathbf{q} = (\pi, \pi)$ the density of states and thus the damping is reduced, leading to sharper peaks in the underdoped case. Experiments [8,34] actually indicate that dispersing ‘spin-wave’ peaks above ω_{res} are better resolved in the more underdoped sample.

VII. EFFECT OF THE COUPLING IN THE DOUBLE-LAYER

So far we have considered a single CuO_2 layer as the most important structural element of cuprate superconductors. However, YBCO and BSCCO contain two coupled CuO_2 planes per unit cell. The observed susceptibility actually follows [8,34,41,95]

$$\chi(\mathbf{q}, q_z, \omega) = \chi^+(\mathbf{q}, \omega) \cos^2\left(\frac{d}{2}q_z\right) + \chi^-(\mathbf{q}, \omega) \sin^2\left(\frac{d}{2}q_z\right)$$

This form reminds of the odd (–) and even (+) linear combination of spin waves in the undoped parent compound [96,97]. \mathbf{q} is the in-plane wave vector as before, d is the distance of the planes within a bi-layer sandwich. We used the single-layer model as an effective model for the odd (‘‘acoustic’’) susceptibility $\chi^-(\mathbf{q}, \omega)$. The experimentally observed neutron spectra in the odd mode, in particular the resonance at $\mathbf{q} = (\pi, \pi)$ and its doping dependence are well reproduced by the single-layer model. Our description of the resonance in $\text{Im}\chi^-((\pi, \pi), \omega)$ does not rely on the bi-layer structure of the material. The important ingredient is the topology of the underlying Fermi surface in combination with the d-wave superconducting state. This has been discussed in detail in Section V above. The even (‘‘optical’’) mode spectrum $\text{Im}\chi^+((\pi, \pi), \omega)$ appears different in experiment. It shows merely a broad peak with dim intensity [8]. In this section the calculation is extended to the bi-layer system. It is shown that the suppression of the resonance in the even mode is mainly a consequence of the inter-plane exchange coupling J^\perp . The odd-mode susceptibility, on the other hand, resembles the one obtained from the single-layer model.

The bi-layer modes have also been explored by averaging the experimentally measured magnetic response over the in-plane Brillouin zone [8,34,41,95],

$$\text{Im}\chi_{2D}^\pm(\omega) = \iint_{-\pi}^{\pi} \frac{d^2q}{(2\pi)^2} \text{Im}\chi^\pm(\mathbf{q}, \omega) \quad (29)$$

After the \mathbf{q} -integration has been performed the odd mode spectrum $\text{Im}\chi_{2D}^-(\omega)$ is still dominated by a sharp resonance; it occurs at the same energy $\omega_{res} \leq 40$ meV as in $\text{Im}\chi^-((\pi, \pi), \omega)$, but with significantly diminished amplitude [8]. In the even (+) mode a second energy scale becomes apparent. $\text{Im}\chi_{2D}^+$ shows no resonance, but a rather broad peak [8,41] or soft onset of spectral weight [34]. The location $\omega_{hump} \sim 80$ meV of this ‘hump’-like structure is almost independent of doping, in contrast to the strongly doping dependent ω_{res} . The ‘hump’ also appears more [41] or less [8] clearly in the odd (–) mode. χ_{2D}^\pm will be studied later in this section. It turns out that particle-hole (ph) excitations across the maximum gap Δ^0 lead to a hump-like peak in both modes in $\text{Im}\chi_{2D}^\pm$, at an energy $\lesssim 2\Delta^0$ almost independent of doping.

A. Results for the bi-layer system

Theoretical expressions for the susceptibility of two coupled planes have been derived in Section II. From Eqs. (22,20) the mode susceptibilities are given by

$$\chi^\pm(\mathbf{q}, \omega) = \frac{\chi_p^{irr}(\omega)}{1 + \tilde{J}^\pm(\mathbf{q})\chi_p^{irr}(\omega)} \quad (30)$$

in units of $(g\mu_B)^2$. χ_p^{irr} is obtained from Eq. (23) with $p \equiv (\mathbf{q}, p_z)$ and $p_z = \{0, \pi\}$ for the modes $\{+, -\}$. The χ^\pm differ in their respective irreducible particle-hole bubble χ_p^{irr} and the effective interaction Eq. (26),

$$\tilde{J}^\pm(\mathbf{q}) = \alpha J(\mathbf{q}) \pm J^\perp, \quad J(\mathbf{q}) = 2J[\cos(q_x) + \cos(q_y)]$$

For the in-plane parameters we take $\alpha = 0.35$, $t = 2J$, $t' = -0.45t$ as before, and for the coupling of the two CuO₂-planes within a bi-layer we chose an antiferromagnetic exchange $J^\perp = 0.2J$ and an inter-plane hopping [45,46]

$$t^\perp(\mathbf{q}) = 2t^\perp[\cos(q_x) - \cos(q_y)]^2 + t_0^\perp$$

with $t^\perp = 0.1t$ and $t_0^\perp = 0$.

We assume an in-plane superconducting order parameter Δ^0 with equal amplitude and phase in both layers. The self-consistent solution of the mean-field equations (19) then leads to a vanishing inter-plane gap $\Delta^{\pm 0} = 0$ (Ref. Eqs. (13,14)) and a very small uRVB amplitude $\hat{\chi}^\perp \approx 0.03$, which has been defined in Eq. (17). Therefore the influence of t^\perp , J^\perp on the fermions that constitute χ_p^{irr} is merely a small splitting of the bandstructure into bonding and anti-bonding bands through the effective inter-plane hopping $\tilde{t}^\perp(\mathbf{k}) \approx xt^\perp(\mathbf{k})$.

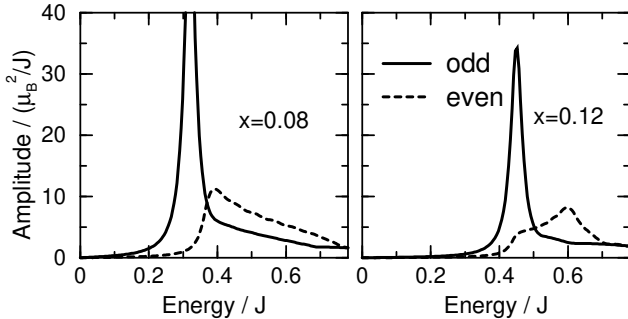


FIG. 13. Odd- and even-mode susceptibility (imag. part) of a bi-layer system, for fixed in-plane wave vector $\mathbf{q} = (\pi, \pi)$. Parameters are $t = 2J$, $t' = -0.45t$, $\alpha = 0.35$, $T = 0$, $4\Gamma = 0.04J \approx 5\text{meV}$ as in the preceding sections, and $J_\perp = 0.2J$, $t_\perp = 0.1t$.

Results for fixed in-plane wave vector $\mathbf{q} = (\pi, \pi)$ are presented in Fig. 13, with ‘experimental’ energy resolution $4\Gamma = 5\text{meV}$. A resonance appears in the odd mode susceptibility, which varies with doping as in the single-layer case. The even mode, on the other

hand, shows a broad peak with much reduced intensity. This is mainly due to the mode-dependent interaction $|\tilde{J}^+(\pi, \pi)| < |\tilde{J}^-(\pi, \pi)|$ in Eq. (30), which shifts the pole in the even (+) mode into the damping continuum. The damping effect is supported by the above-mentioned splitting of fermion bands. It should be emphasized that the resonance in the even mode is not totally suppressed, but shifted and strongly damped. In experiment [8] a similar observation has been made.

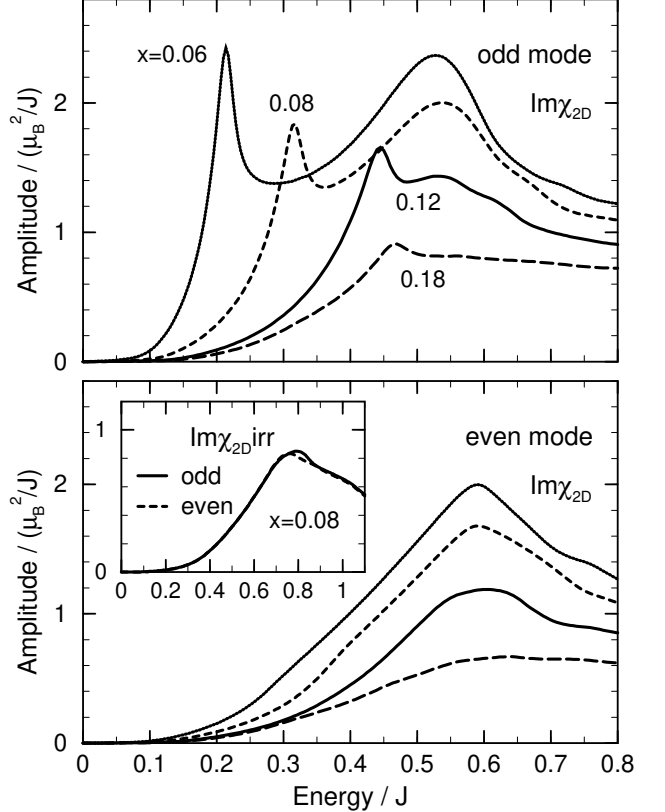


FIG. 14. Wave-vector \mathbf{q} integrated odd- and even-mode susceptibilities $\text{Im}\chi_{2D}$ from Eq. (31) for hole filling $x = 0.06 \dots 0.18$. Parameters as in Fig. 13. **Inset:** \mathbf{q} -integrated bubble spectrum $\text{Im}\chi_{2D}^{irr}$ for $x = 0.08$. The maximum is located close to $2\Delta^0 = 0.78J$.

A new feature appears if we look at the wave-vector integrated susceptibility Eq. (29), which is shown in Fig. 14. Similar to the case of fixed $\mathbf{q} = (\pi, \pi)$ a resonance appears only in the odd mode. It appears at the same position as in $\text{Im}\chi^-(\pi, \pi)$ with the same strong doping dependence. Additionally, both modes $\text{Im}\chi_{2D}^\pm(\omega)$ show a broad peak (‘hump’) at an energy somewhat below $2\Delta^0$, almost independent of doping ($2\Delta^0 \approx 0.78J$ for $x = 0.08$). For an explanation of this ‘hump’ we first go back to the single-layer case: The spectrum $\text{Im}\chi^{irr}(\mathbf{q}, \omega)$ of the irreducible ph-bubble shown in Fig. 11 (bottom) is dominated by peaks around $2\Delta^0$. These van Hove singularities (v.H.s.) follow the quite flat \mathbf{q} -space dispersion shown in Fig. 12. When the wave-vector is integrated

over in $\text{Im}\chi_{2D}^{irr}(\omega) = \iint_{-\pi}^{\pi} \frac{d^2q}{(2\pi)^2} \text{Im}\chi^{irr}(\mathbf{q}, \omega)$, the v.H.s. contribute a large density of states, leading to a broad peak with maximum at $\omega = 2\Delta^0$. This argument extends to the bi-layer system: The hump appears almost identically in both modes of the bubble $\text{Im}\chi_{2D}^{\pm irr}(\omega)$, which is shown in the inset of Fig. 14. Its position follows $2\Delta^0$ to slightly higher energies for reduced doping level x .

When the final-state interaction Eq. (30) is switched on in the odd ($-$) mode, the resonance appears (see Fig. 14 top). Since spectral weight is shifted to lower energies, the hump is relocated to an x -independent position below $2\Delta^0$. The even ($+$) mode (Fig. 14 bottom) experiences a weaker renormalization through Eq. (30), no resonance is formed, and its hump is relocated less strongly. Recent FLEX calculations for a 3-band single-layer Hubbard model in the overdoped regime [26] give results for $\text{Im}\chi_{2D}(\omega)$ comparable to our odd mode susceptibility.

The intensity of the resonance in $\text{Im}\chi_{2D}^-(\omega)$ is much reduced from its value in $\text{Im}\chi^-(\pi, \pi, \omega)$ measured at fixed wave vector. Therefore in $\text{Im}\chi_{2D}$ the resonance at ω_{res} and the excitations across the maximum gap at $\omega_{hump} \lesssim 2\Delta^0$ are of comparable intensity and can both be observed experimentally. This is due to the fact that the latter occupy a large part of the in-plane Brillouin zone (BZ), while the resonance is just a narrow peak in \mathbf{q} -space. Despite its large amplitude, the resonance contributes only little to Eq. (29). For the actual computation of $\text{Im}\chi_{2D}^{\pm}$ we used wave-vector scans [98] in $(\pi, 0)$ -direction like those shown in Fig. 9 (extended to the whole BZ) and assumed [99] a susceptibility isotropic around (π, π) , i.e.,

$$\chi_{2D}^{\pm}(\omega) = \frac{1}{2\pi} \int_0^{\pi} k dk \chi^{\pm}(\mathbf{q}, \omega), \quad \mathbf{q} = (\pi + k, \pi) \quad (31)$$

The resonance is actually so sharp in \mathbf{q} -space (see Fig. 9) that it does not become visible in the resulting $\text{Im}\chi_{2D}^-(\omega)$. For each ω the respective \mathbf{q} -scan has therefore been convoluted with a Gaussian of FWHM = 0.25 r.l.u. = 0.5π , in order to simulate a finite instrumental wave-vector resolution. Application of Eq. (31) then leads to the curves shown in Fig. 14.

B. Comparison to experiment

Two experimental groups studied the wave-vector integrated magnetic response $\text{Im}\chi_{2D}^{\pm}$ in underdoped YBCO. Refs. [41,95] reported a lineshape for YBCO_{6.6} which agrees quite well with the theoretical result Fig. 14 for $x \leq 0.08$. A ‘hump’ in $\text{Im}\chi_{2D}^+$ (even) appears at ≈ 100 meV, $\text{Im}\chi_{2D}^-$ (odd) shows a similar structure at a somewhat lower energy ≈ 90 meV. The well-known resonance appears only in $\text{Im}\chi_{2D}^-$, at 34 meV. In Refs. [8,34] two underdoped samples YBCO_{6.7} and YBCO_{6.5}

have been studied. In the even (“optical”) mode of YBCO_{6.7} a hump appears around 70 meV, whereas the odd (“acoustic”) mode shows a weak hump-like structure at ≈ 55 meV, separated from the resonance at 33 meV. In the more underdoped sample YBCO_{6.5} these features tend to move up in energy, while the resonance in $\text{Im}\chi_{2D}^-$ shifts down to 25 meV.

Although the detailed experimental lineshapes are not unique [100], the qualitative features of our calculation are found in the neutron-scattering spectra. In particular we obtain the different dependence on doping level of the resonance at ω_{res} in the odd mode and the hump-like feature at ω_{hump}^{\pm} in both modes. Also is ω_{hump}^- of the odd mode lower than the ω_{hump}^+ of the even mode. Theory and experiments can also partly be compared quantitatively. The measured neutron-scattering intensities [8,41] are of the same order as the theoretical ones in Fig. 14 (using $J = 120$ meV, i.e., $1\mu_B^2/J = 8.3\mu_B^2/eV$). The maximum of the hump in the even, odd mode in Fig. 14 occurs at $\omega^{+,-} \approx 0.6J, 0.53J = 72$ meV, 64 meV, in good agreement with the measurements [8] on YBCO_{6.7} at low temperature. Note that the maximum gap $\Delta^0 = 30 - 45$ meV [5] is consistent to the value from the mean-field calculation (see Section II), $2\Delta^0$ is the upper limit for the hump position in Fig. 14.

C. Discussion

The wave-vector integrated magnetic response in underdoped systems is characterized by two energy scales with opposite dependence on the doping level. The first is the position ω_{res} of the “41 meV resonance”, which appears in the odd ($-$) mode for fixed wave vector $\mathbf{q} = (\pi, \pi)$ as well as in the \mathbf{q} -integrated susceptibility. It moves down in energy when doping x is reduced and becomes a Bragg peak at the transition to the AF ordered state at $x = x_c$. The second is essentially the maximum gap Δ^0 , which increases with reduced x . It determines the position ω_{hump} of the additional broad peak (‘hump’). The latter appears in both bi-layer modes, but only if the in-plane wave-vector is integrated over. The hump is caused by particle-hole excitations across $2\Delta^0$, and is pulled down somewhat by the final-state interaction Eq. (30). It should be noted that it is very robust against a variation of the next-nearest-neighbor hopping t' , i.e., the topology of the fermion’s band structure and Fermi surface. Whereas the resonance vanishes for $t' = 0$ the hump remains almost unaffected. The mechanism is very much different from the optical spin waves that appear in the undoped $x = 0$ bi-layer system if a finite Néel order parameter is taken into account. Therefore the appealing similarity of the hump- (or threshold-like) feature in the superconducting YBCO samples and the optical spin-wave gap seen in the undoped parent com-

pound [97] is accidental.

VIII. SUMMARY AND OUTLOOK

This paper presented a theory for the magnetic excitation spectrum of $\text{YBa}_2\text{Cu}_3\text{O}_{6+y}$ (YBCO) and $\text{Bi}_2\text{Sr}_2\text{CaCu}_2\text{O}_{8+\delta}$ (BSCCO) superconductors. We considered the so-called “41 meV resonance” at fixed in-plane wave vector $\mathbf{q} = (\pi, \pi)$, the magnetic response in \mathbf{q} -space, the peculiarities due to the bi-layer structure of YBCO and BSCCO, and the local (\mathbf{q} -integrated) susceptibility. Most of the results are in good agreement with the neutron-scattering experiments. The resonance is obtained as a collective spin-1 excitation in the superconducting and spin-gap states (the latter corresponding to the pseudo-gap regime of cuprates). Its energy scale and spectral weight as function of the doping level x at low temperature are satisfactorily reproduced. The absence of damping in optimally doped systems is caused by the d-wave superconducting gap in connection with the hole-type topology of the underlying Fermi surface. The bi-layer structure is not necessary for the resonance to form in the odd-mode (acoustic) susceptibility. The mere effect of the finite inter-layer coupling J^\perp is an almost suppression of the resonance in the even (optical) mode. The observed pattern of incommensurate peaks in \mathbf{q} -space has been traced back to a dynamic nesting effect of the d-wave superconductor, and the peak’s dispersion has been derived for optimally and underdoped systems. Besides the resonance a second, hump-like feature appears in the wave-vector integrated magnetic spectrum. It is caused by particle-hole excitations across the maximum gap Δ^0 that occupy a large area in the 2D Brillouin zone. Their energy $\omega_{hump} \lesssim 2\Delta^0$ is almost independent of hole filling, in strong contrast to the resonance position ω_{res} . Also is this hump insensitive to the Fermi-surface topology.

A salient property of the resonance at (π, π) is the variation of its energy ω_{res} with hole filling x . The t - J -model, i.e., the doped Mott insulator naturally provides the energy scales for the resonance in the underdoped and overdoped regimes: The mean-field theory describes magnetic excitations in terms of quasi particles (QP) (the fermions) with a Fermi velocity $\tilde{v}_F \approx (x + 0.15J/t)v_F$ reduced from the bare parameter. Hence in underdoped systems the QP’s chemical potential is smaller than the gap, $|\mu^f| < \Delta^0$, and determines the scale for the resonance energy as $\omega_{res} \lesssim 2|\mu^f|$ (see Fig. 7). Thus ω_{res} is found to increase with hole filling x , in accordance with experiment. In the overdoped regime, on the other hand, we have $|\mu^f| \gg \Delta^0$, and the resonance $\omega_{res} \lesssim 2\Delta^0$ is connected to the gap which decreases with x .

The mean-field theory in its present form overestimates the antiferromagnetic (AF) state in the phase diagram.

Therefore we had to introduce the phenomenological parameter α , which reduces the interaction $J \rightarrow \alpha J$ in the spin-flip particle-hole channel Eq. (24) of the quasi particles. The present study shows that already the simplest model $\alpha(\mathbf{q}, \omega, x) = \alpha$ leads to consistent results for neutron-scattering spectra and magnetic correlation length $\xi_{AF}(x)$ in the relevant range of doping, energy, and wave vector. With respect to the doping dependence of ω_{res} and ξ_{AF} this is due to the above-mentioned renormalization of the QP. In the half-filled case $x = 0$, which we did not consider here, the mean-field theory delivers a Néel state with the correct spin-wave velocity only if J is kept unrenormalized, i.e., $\alpha(x = 0) = 1$. With doping the AF state is destroyed by the propagation of holes in the spin background [66,71,72]. We expect that a refined theory, where these processes are included as corrections to mean field, yields an $\alpha(x)$ which decreases quickly in the AF region $x < x_c$ and then levels off in the paramagnetic (superconducting) phase $x > x_c$. This is subject to future work.

We thank P. Wölfle for useful comments on the manuscript. This work has been supported by the NSF under MRSEC Program No. DMR 98-08941 and the Deutsche Forschungsgemeinschaft through SFB 195.

-
- [1] J. Rossat-Mignod *et al.*, *Physica B* **169**, 58 (1991).
 - [2] H. A. Mook *et al.*, *Phys. Rev. Lett.* **70**, 3490 (1993).
 - [3] H. F. Fong *et al.*, *Phys. Rev. Lett.* **75**, 316 (1995).
 - [4] P. Bourges, L. P. Regnault, L. Sidis, and C. Vettier, *Phys. Rev. B* **53**, 876 (1996).
 - [5] ARPES measurements on untwinned YBCO_{6.995} reported in Ref. [101] are consistent with maximum gap values $\Delta^0 = 29$ meV and 44 meV at $(\pi, 0)$ (X-point) and $(0, \pi)$ (Y-point).
 - [6] P. Dai *et al.*, *Phys. Rev. Lett.* **77**, 5425 (1996).
 - [7] H. F. Fong, B. Keimer, D. L. Milius, and I. A. Aksay, *Phys. Rev. Lett.* **78**, 713 (1997).
 - [8] H. F. Fong *et al.*, *Phys. Rev. B* **61**, 14773 (2000).
 - [9] P. Dai, H. A. Mook, R. D. Hunt, and F. Doğan, *Phys. Rev. B* **63**, 054525 (2001).
 - [10] H. F. Fong *et al.*, *Nature* **398**, 588 (1999).
 - [11] H. He *et al.*, *Phys. Rev. Lett.* **86**, 1610 (2001).
 - [12] J. Mesot *et al.*, (2001), preprint cond-mat/0102339.
 - [13] T. Tanamoto, K. Kuboki, and H. Fukuyama, *J. Phys. Soc. Jpn.* **60**, 3072 (1991).
 - [14] T. Tanamoto, H. Kohno, and H. Fukuyama, *J. Phys. Soc. Jpn.* **63**, 2739 (1994).
 - [15] Y. Zha, K. Levin, and Q. Si, *Phys. Rev. B* **47**, 9124 (1993).
 - [16] D. Z. Liu, Y. Zha, and K. Levin, *Phys. Rev. Lett.* **75**, 4130 (1995).
 - [17] G. Stemmann, C. Pépin, and M. Lavagna, *Phys. Rev. B* **50**, 4075 (1994).

- [18] F. Onufrieva and J. Rossat-Mignod, Phys. Rev. B **52**, 7572 (1995).
- [19] K. Maki and H. Won, Phys. Rev. Lett. **72**, 1758 (1994).
- [20] I. I. Mazin and V. M. Yakovenko, Phys. Rev. Lett. **75**, 4134 (1995).
- [21] N. Bulut and D. J. Scalapino, Phys. Rev. B **53**, 5149 (1996).
- [22] M. I. Salkola and J. R. Schrieffer, Phys. Rev. B **58**, R5944 (1998).
- [23] M. R. Norman, Phys. Rev. B **63**, 092509 (2001).
- [24] C.-H. Pao and N. E. Bickers, Phys. Rev. B **51**, 16310 (1995).
- [25] T. Dahm, D. Manske, and L. Tewordt, Phys. Rev. B **58**, 12454 (1998).
- [26] T. Takimoto and T. Moriya, J. Phys. Soc. Jpn. **67**, 3570 (1998).
- [27] A. Abanov and A. V. Chubukov, Phys. Rev. Lett. **83**, 1652 (1999).
- [28] D. K. Morr and D. Pines, Phys. Rev. Lett. **81**, 1086 (1998).
- [29] E. Demler and S. C. Zhang, Phys. Rev. Lett. **75**, 4126 (1995).
- [30] S. C. Zhang, Science **275**, 1089 (1997).
- [31] J. Brinckmann and P. A. Lee, J. Phys. Chem. Solids **59**, 1811 (1998), (= cond-mat/9710065).
- [32] O. Tschernyshyov, M. R. Norman, and A. V. Chubukov, Phys. Rev. B **63**, 144507 (2001).
- [33] B. J. Sternlieb *et al.*, Phys. Rev. B **50**, 12915 (1994).
- [34] P. Bourges *et al.*, Phys. Rev. B **56**, R11439 (1997).
- [35] H. A. Mook *et al.*, Nature **395**, 580 (1998).
- [36] M. Arai *et al.*, Phys. Rev. Lett. **83**, 608 (1999).
- [37] P. Bourges *et al.*, Science **288**, 1234 (2000).
- [38] H. A. Mook, P. Dai, F. Doğan, and R. D. Hunt, Nature **404**, 729 (2000).
- [39] T. E. Mason *et al.*, Phys. Rev. Lett. **71**, 919 (1993).
- [40] K. Yamada *et al.*, Phys. Rev. Lett. **75**, 1626 (1995).
- [41] P. Dai *et al.*, Science **284**, 1344 (1999).
- [42] J. Brinckmann and P. A. Lee, Phys. Rev. Lett. **82**, 2915 (1999).
- [43] R. P. Feynman, *Statistical Mechanics* (Addison Wesley, Reading, Massachusetts, 1972).
- [44] The Feynman variation principle provides a unique decomposition of the two-particle interaction S^J , taking into account all different ways of decoupling S^J into quadratic terms. Alternatively a saddle-point approximation using Hubbard–Stratonovich (HS) fields has been used [56]. Here one has to write $S^J = g_{ph}S^J + \bar{g}_{ph}S^J + g_{pp}S^J$ in the action, in order to decouple S^J in three channels (ways) using three HS fields. Different choices of weight factors which satisfy $g_{ph} + \bar{g}_{ph} + g_{pp} = 1$ lead to different saddle-point approximations which do not coincide with the variation principle. In particular the numerical coefficients in Eq. (9) are different from those in Ref. [56]. However, the approximation for paramagnetic phases discussed in Ref. [56] is qualitatively similar to ours.
- [45] S. Chakravarty, A. Sudbø, P. W. Anderson, and S. Strong, Science **261**, 337 (1993).
- [46] O. K. Andersen, O. Jepsen, A. I. Lichtenstein, and I. I. Mazin, Phys. Rev. B **49**, 4145 (1994).
- [47] Note that in Ref. [42] slightly different units have been used: $\chi^{meas} = (g\mu_B)^2\chi/2$, with an irred. part $\chi^0 = 2\chi^{irr}$.
- [48] G. Baskaran, Z. Zou, and P. W. Anderson, Sol. State Comm. **63**, 973 (1987).
- [49] A. E. Ruckenstein, P. J. Hirschfeld, and J. Appel, Phys. Rev. B **36**, 857 (1987).
- [50] G. Kotliar and J. Liu, Phys. Rev. B **38**, 5142 (1988).
- [51] Y. Suzumura, Y. Hasegawa, and H. Fukuyama, J. Phys. Soc. Jpn. **57**, 401 (1988).
- [52] I. Affleck and J. B. Marston, Phys. Rev. B **37**, 3774 (1988).
- [53] P. W. Anderson, Science **235**, 1196 (1987).
- [54] H. Fukuyama, Prog. Theoret. Phys. Suppl. **108**, 287 (1992).
- [55] N. Nagaosa and P. A. Lee, Phys. Rev. B **45**, 966 (1992).
- [56] M. U. Ubbens and P. A. Lee, Phys. Rev. B **46**, 8434 (1992).
- [57] L. B. Ioffe and A. I. Larkin, Phys. Rev. B **39**, 8988 (1989).
- [58] Y. J. Uemura *et al.*, Phys. Rev. Lett. **62**, 2317 (1989).
- [59] C. Renner *et al.*, Phys. Rev. Lett. **80**, 149 (1998).
- [60] N. Miyakawa *et al.*, Phys. Rev. Lett. **80**, 157 (1998).
- [61] A. G. Loeser *et al.*, Science **273**, 325 (1996).
- [62] H. Ding *et al.*, Nature (London) **382**, 51 (1996).
- [63] X. G. Wen and P. A. Lee, Phys. Rev. Lett. **76**, 503 (1996).
- [64] P. A. Lee, N. Nagaosa, T.-K. Ng, and X.-G. Wen, Phys. Rev. B **57**, 6003 (1998).
- [65] I. Affleck, Z. Zou, T. Hsu, and P. W. Anderson, Phys. Rev. B **38**, 745 (1988).
- [66] T. K. Lee and S.-P. Feng, Phys. Rev. B **38**, 11809 (1988).
- [67] C. Gros, Ann. Phys. (N.Y.) **189**, 53 (1989).
- [68] M. Inui, S. Doniach, P. J. Hirschfeld, and A. E. Ruckenstein, Phys. Rev. B **37**, 2320 (1988).
- [69] M. Inaba, H. Matsukawa, M. Saitoh, and H. Fukuyama, Physica C **257**, 299 (1996).
- [70] D. H. Kim and P. A. Lee, Ann. Phys. (N.Y.) **272**, 130 (1999), also as cond-mat/9810130.
- [71] J. Igarashi and P. Fulde, Phys. Rev. B **45**, 12357 (1992).
- [72] G. Khaliullin and P. Horsch, Phys. Rev. B **47**, 463 (1993).
- [73] T. R. Thurston *et al.*, Phys. Rev. B **40**, 4585 (1989).
- [74] R. R. P. Singh and R. L. Glenister, Phys. Rev. B **46**, 11871 (1992).
- [75] M. H. Schabel *et al.*, Phys. Rev. B **57**, 6107 (1998).
- [76] B. Keimer *et al.*, Physica C **282–287**, 232 (1997).
- [77] For hole filling below $x_c = 0.023$ the mean-field theory and therefore Fig. 7 is not valid, since a finite magnetic order parameter is not contained. The limit $x \rightarrow 0$ here reproduces the π -flux phase [52], with nodes at $(\pm\pi/2, \pm\pi/2)$ in the fermion dispersion, leading to $\Omega_0 \rightarrow 0$.
- [78] In an approach based on quasi particles the susceptibility is given by the same RPA formula Eq. (24), with the (assumed) effective interaction replacing $2J[\dots]$.
- [79] See, e.g., Ref. [102].
- [80] P. Dai, H. A. Mook, and F. Doğan, Phys. Rev. Lett. **80**, 1738 (1998).
- [81] P. Bourges, B. Keimer, L. P. Regnault, and Y. Sidis, J. Supercond. **13**, 735 (2000).

- [82] J. P. Lu, Phys. Rev. Lett. **68**, 125 (1992).
- [83] Note that in Ref. [42] and some experimental work $\delta \equiv 2\delta_x$ is used.
- [84] B. Lake *et al.*, Nature **400**, 43 (1999).
- [85] H. J. Schulz, Phys. Rev. Lett. **64**, 1445 (1990).
- [86] P. B. Littlewood, J. Zaanen, G. Aeppli, and H. Monien, Phys. Rev. B **48**, 487 (1993).
- [87] When x is reduced the bubble spectrum at the threshold Ω_0 changes from step like $\sim \Theta(\omega - \Omega_0)$ to $\sim \sqrt{\omega - \Omega_0}$ (comp. Sect. V), which leads to an almost immediate damping of the resonance when \mathbf{q} moves off (π, π) .
- [88] J. Zaanen and O. Gunnarson, Phys. Rev. B **40**, 7391 (1989).
- [89] D. Poilblanc and T. M. Rice, Phys. Rev. B **39**, 9749 (1989).
- [90] H. J. Schulz, J. Phys. (Paris) **50**, 2833 (1989).
- [91] Y.-J. Kao, Q. Si, and K. Levin, Phys. Rev. B **61**, R11898 (2000).
- [92] J.-X. Li and C.-D. Gong, (2001), preprint cond-mat/0103456.
- [93] F. Onufrieva and P. Pfeuty, (1999), preprint cond-mat/9903097.
- [94] D. Manske, I. Eremin, and K. H. Bennemann, Phys. Rev. B **63**, 054517 (2001).
- [95] S. M. Hayden *et al.*, Physica B **241–243**, 765 (1998).
- [96] J. M. Tranquada *et al.*, Phys. Rev. B **40**, 4503 (1989).
- [97] S. M. Hayden *et al.*, Phys. Rev. B **54**, R6905 (1996).
- [98] This procedure is similar to the one used in the experimental study Ref. [8]. Use of wave-vector scans in directions other than $(\pi, 0)$ causes only minor changes in our results.
- [99] The resonance is in fact isotropic around (π, π) , for the excitations around $2\Delta^0$ this is an acceptable model.
- [100] We suggest that this is (at least partly) due to different procedures used for subtracting an energy dependent background. In the theoretical calculation a subtraction of a background from the wave-vector scans leads to a reduction of intensity and change in shape of the ‘hump’, while the resonance is not affected. The background is assumed constant throughout the Brillouin zone and is determined for each energy as the minimum of the wave-vector scan in $(\pi, 0)$ direction. Fig. 14 is computed from the unsubtracted (bare) scans as described in the text.
- [101] D. H. Lu *et al.*, Phys. Rev. Lett. **86**, 4370 (2001).
- [102] H.-Y. Kee and Y. B. Kim, Phys. Rev. B **59**, 4470 (1999).